2019

# 3D printing of chitosan-based scaffolds for wound healing

Sulokshana Marks
*University of Wollongong*

UNIVERSITY OF WOLLONGONG AUSTRALIA

# 3D printing of chitosan-based scaffolds for wound healing


By

**Sulokshana Marks**

Bachelor of Chemistry (Hons)

Supervisors:
Prof Gordon G Wallace
Dr Zhilian Yue
Prof Michael J Higgins

Clinical advisor:
Assoc. Prof Chris Baker


This thesis is presented as part of the requirement for the conferral of the degree:

**MASTER OF PHILOSOPHY**

From


**The University of Wollongong**

AUSTRALIAN INSTITUTE OF INNOVATIVE MATERIALS

INTELLIGENT POLYMER RESEARCH INSTITUTE


August 2019

# Certification

I, Sulokshana Marks, declare that this thesis submitted in fulfilment of the requirements for the conferral of the degree, Master of Philosophy (Biofabrication), within the AIIM Faculty at the Intelligent Polymer Research Institute from the University of Wollongong, is wholly my own work unless otherwise referenced or acknowledged. This document has not been submitted for qualifications at any other academic institution.

Sulokshana Marks
26th August 2019

# Acknowledgments

There are many people that have earned my gratitude for their contribution and whom without this thesis would not have been possible. First and foremost, I would like to acknowledge my indebtedness and render my warmest thanks to my supervisor, Dr Zhilian Yue for her kind guidance and expert advice that have been invaluable throughout all stages of this work. Not only as my teacher but also as my she taught me more than I could ever give her credit for and showed me by example what it takes to be a good scientist. I take pride acknowledging the insightful guidance and perspicacity of Prof Gordon Wallace. It's always been such a strength knowing that someone who is an esteemed innovator is always there to steer me in the right direction. I also take this opportunity to thank Prof Michael Higgins for coordinating the Masters in Biofabrication program from day one; getting selected for this program became a turning point in my life. Special thanks go to Dr Chee Too for proofreading this thesis in such a short time period.

My sincere thanks also go to my collaborator, Assoc. Prof Chris Baker, a Melbourne-based Dermatologist for his valuable contribution to match my work with the real-world application. Besides my advisors, this work would not have been achievable without the deep insight and help from the expertise in the tools and training from especially Dr. Sepidar Sayyar, Dr. Johnson Chung, Dr Patricia Hayes, Dr Kerry Gilmore and Dr Sanjeev Gambhir.

I am grateful to all of those whom I had the pleasure of working with throughout my project; for their continuous support and creating a friendly atmosphere in the middle of all the research chaos. Special thanks go to Xifang Chen, Yucho Fan, Lingzhi Khan, Thomas Robbinson and Jeremy Nicolas Dinoro.

My acknowledgement would be incomplete without thanking the biggest source of my strength, my family. Mom, Dad and my loving husband Udara, thank you for always believing in me with so much love, continuous patience and endless support, without which I wouldn't have come this far. My brother Vinodh who I always look up to when I got lost in this far away land. Finally, to my friends whom I called my homebodies, you know who you are and thanks for all the encouragements and always making me confident just the way I am.

# ABSTRACT

3D printing has made a significant breakthrough in the field of tissue engineering; mainly due to its possibility to create scaffolds with more control over spatial arrangement and ability to manufacture patient specific replacements. The lack of different biomaterial inks that can fulfil the requirements of both additive manufacturing and specific biological requirements is a major bottleneck that limits the potential of this technique for clinical translation. Herein, we present the development of ink formulations based on a photo-curable chitosan for 3D printing of scaffolds for wound healing application.

Chitosan, a linear polysaccharide well-established for wound healing application, was modified into a water soluble and photo-curable form, namely methacryloyl chitosan (ChiMA). The product was characterised by FTIR and $^{1}$HNMR. A range of ChiMA/MC inks were formulated for extrusion printing in which methyl cellulose (MC) serves as a rheological modifier. These ink formulations were subjected to several screening tests, including an extrudability test and a semi-quantitative assessment of printability, to identify the appropriate combinations of CHiMA and MC for further extrusion printing studies. Physicochemical properties of the crosslinked form of the inks (hydrogels) were characterised as part of the screening test to establish a correlation between ink composition and concentration on the final scaffold. Based on the screening results, 2%ChiMA/3%MC and 3%ChiMA/2%MC inks were selected as the lead ink formulations for rheological studies. It was found that both the selected inks had a yield stress less than 350 Pa, a value well below the plug-flow regime of 1866 Pa, which also demonstrated excellent shear thinning properties upon being extruded through the nozzle. Self-recovery data proved the inks' ability for regaining structural integrity following printing, thus confirming their utilization as feeding inks for extrusion-based 3D printing.

Further, the rheological data of the selected inks was fitted into a previously developed mathematical model to determine the bioprinting window. The bioprinting window can be defined as a selection of a range which falls within operating capabilities of the bioprinter based on calculated average extrusion velocity. This model was also used to understand the extrusion behaviour in terms of extrusion velocity, shear stress, shear rate and resistance time of the biomaterial ink inside the nozzle. This model was used as a tool to optimize a biomaterial ink for the bioprinter within its operating parameters and to minimize the trial and error approach. Evaluation of the printed structures was carried out by measuring the strut diameter with respect

to varying printing speed under the same extrusion pressure, and reproduction of different shapes. Several types of printed structures including mesh, circular shape and star shape were achieved. These results elucidated that the 3%ChiMA/2%MC ink formulation has better resolution than the 2%ChiMA/3%MC ink formulation. Preliminary cytocompatibility studies revealed that the 3D printed structures did not exert significant cytotoxic effect on human dermal fibroblast. However, the printed structures did not support cell attachment and proliferation. This suggests, as demonstrated by a pilot collagen coating study, that further modification with appropriate cell adhesion motifs is required in future studies in order to improve the performance of 3D printed scaffolds as cellular support for wound healing applications. The scheme of this present work is illustrated in Figure 1.

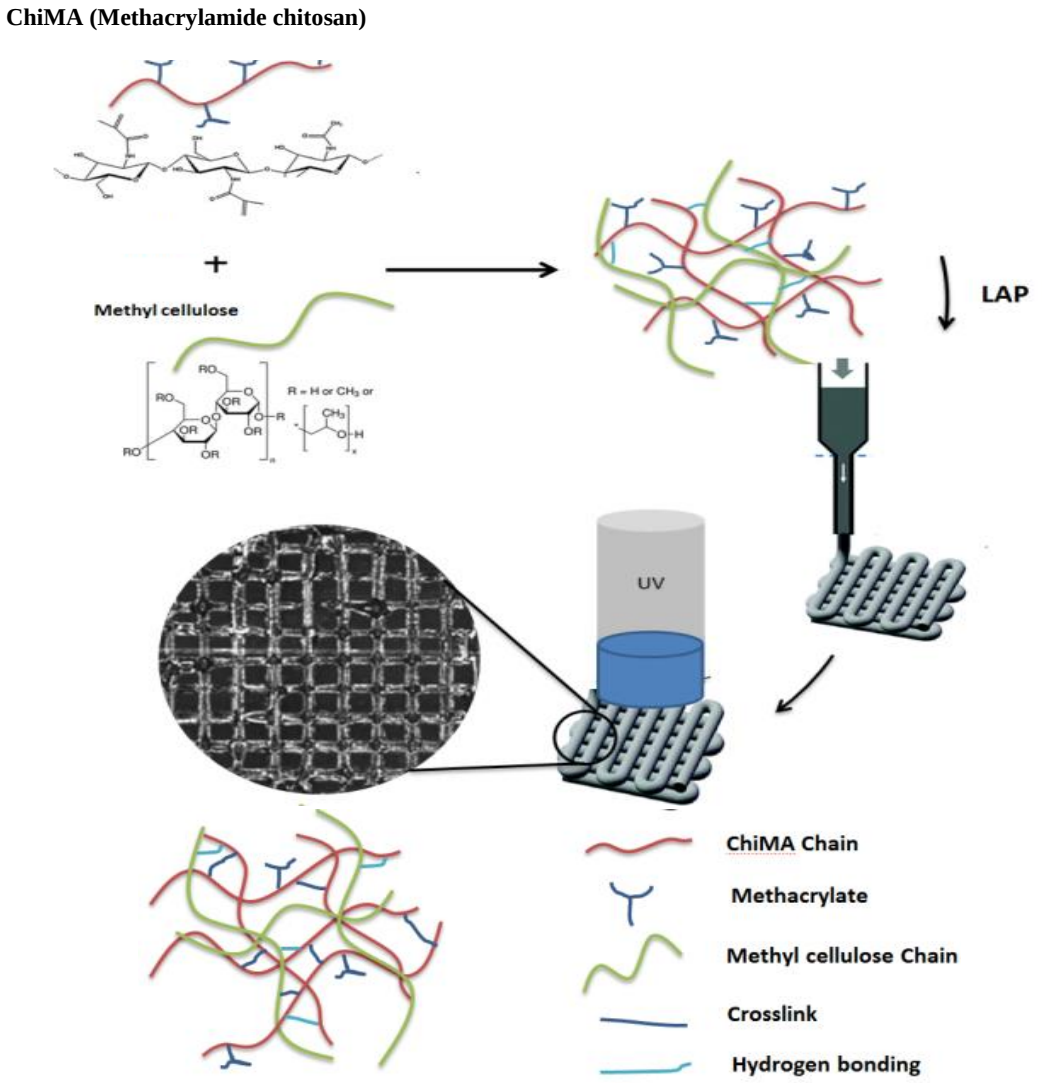


**Figure 1. Schematic representation of ChiMA (methacrylamide chitosan)/methyl cellulose biomaterial ink development.**

# Contents

# List of Figures

# Abbreviations

**ChiMA** Methacrylamide chitosan

**MC** Methyl cellulose

**LAP** Lithium phenyl-2,4,6-trimethylbenzoylphosphinate

# List of Tables

# 1. INTRODUCTION

This thesis focusses on the development of biomaterial ink formulations based on a photo-curable chitosan for 3D printing of scaffolds to be used in wound healing applications. In this chapter, the anatomy of skin, the wound healing process, current treatment options and their limitations are introduced. To address the development of new strategies for wound healing, the area of bioprinting is then introduced including the additive manufacturing methods and biomaterial inks that are available. This is followed by the material consideration from chemical and physiological perspectives, including modification of the materials. Lastly, the aims and objectives of the current work are presented.

## 1.1. The Skin

Human skin is the outermost covering layer and largest multifunctional organ of the body. Thorough knowledge of its structure and function is essential when dealing with the development of bioengineered skin constructs. It acts as the main interaction site with the surroundings while affording multifunction such as protection, thermoregulation, metabolism, sensation, and synthesis of vitamin D. Healthy skin can be divided into three main layers: (from top to bottom) the epidermis, dermis and hypodermis (Figure 1.1). The epidermis is the topmost layer with 95% of it being composed of keratinocytes and the remainder of cell types including being Melanocytes, Langerhans cells and Merkel cells (Freinkel and Woodley 2001). Keratinocytes continuously differentiate in a basal to superficial direction and this is known as keratinization a process that approximately takes up to six weeks for the cells to reach the skin surface where they are finally shed. (Freinkel and Woodley 2001, You, Eames et al. 2017). Dermis is the more profound layer of the skin which lies beneath the epidermis. It contains various cellular elements: fibroblasts, mast cells; supporting matrix: collagen, elastin, a

network of capillaries, and nerves. The dermis also contains a number of specialized cells including hair follicles, sweat glands, and sebaceous glands. The major cell type present in the dermis is fibroblast and it plays a major role in the wound healing process by producing remodelling enzymes such as proteases and collagenases (Metcalfe and Ferguson 2007). The lowermost subcutaneous fat layer is also known as hypodermis and it consists of loose connective tissue, elastin, and cells such as fibroblasts, macrophages and adipocytes. This layer plays a central role in regulating the body's temperature, acting as an energy source and attaching the dermis to the muscles and bones.

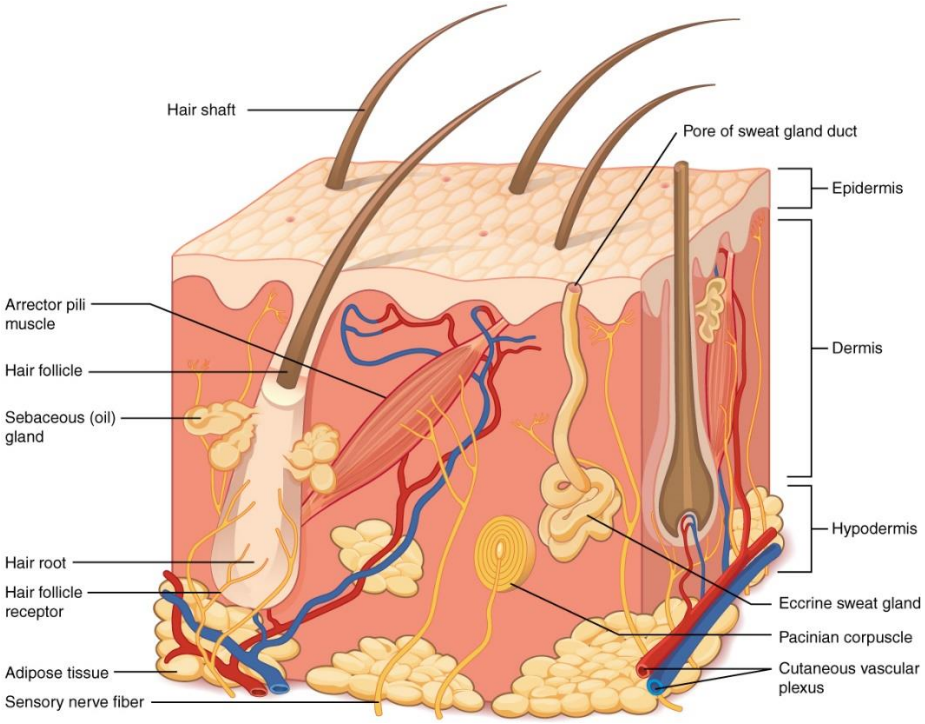


**Figure 1.1 Anatomical structure of human skin (Collage 2014).**

## 1.2.Wounds

A wound can be described as a disruption of the anatomic and physiologic continuity of the skin caused by accidents and injuries or as a result of underlying medical or physiological condition. Even though the wound healing cascade triggers naturally, in some circumstances it

fails to complete or takes a longer time frame due to complications associated with one or more of the stages of wound healing such as oxygenation, infection, age and sex hormones, stress, diabetes, obesity, medications, alcoholism, smoking, and nutrition (Guo and DiPietro 2010). When a wound fails to progress through the normal stages of healing thus cannot be repaired in an orderly and timely manner with obtaining a sufficient anatomic and functional integrity creates a chronic wound (Lazarus, Cooper et al. 1994). According to the 2018 statistics, over 400,000 people in Australia suffer from chronic wounds costing the health care system around 3 billion dollars annually, apart from the indirect costs associated with further wound management (Pacella 2017). On the other hand, apart from the burden of the chronic wounds, the next biggest problem associated with the wound is skin scarring. Unlike the normal skin, scar tissue has a lower functional quality due to the preclusion of rearrangement of new proteins (mainly collagen) in an orderly manner similar to normal skin. Instead the proteins are arranged in a more random and mismatched way with excessive extra-cellular matrix (Yates, Hebda et al. 2012). Scarring can be in a broad spectrum ranging from "normal" to more problematic excessive scarring; including pathological scar formation like keloid and hypertrophic scarring (Marshall, Hu et al. 2018). Just like chronic wounds, scarring can affect the overall health and wellbeing of a person; causing social stigma and physiological trauma (Bayat, McGrouther et al. 2003).

### 1.2.1. Wound healing

The wound healing process is triggered instantly when damage happens to the skin, with the primary aim of achieving the healing in the minimal amount of time and secondary aim of reducing scar tissue formation. The whole wound healing process can be divided into three interrelated and highly programmed phases: inflammation, proliferation, and remodelling (Figure 1.2)

Haemostasis is the immediate response of the body after an injury, resulting in clot formation and platelet aggregation to limit further blood loss (Enoch and Leaper 2008). These platelets are crucial in the wound healing cascade as they not only trigger the coagulation but also produce chemotactic factors, including platelet-derived growth factor (PDGF) and transforming growth factor-b (TGF-b) for the subsequent stages in the healing process (Morton and Phillips 2016). The main purpose of the inflammatory phase is to achieve a good environment for the healing by cleansing the debris and bacteria. There are two predominant cells in this phase: neutrophils and macrophages. As Diegelmann et al. have described, the functions of neutrophils are to remove foreign material, bacteria and non-functional host cells and damaged matrix components that could be present at the wound site (Diegelmann and Evans 2004). Macrophage cells are responsible for phagocytosis of pathogenic organisms, degrading wound debris, and stimulating granulation tissue formation and angiogenesis. Singh, S et al (2017) have stated that the inflammatory phase persists in making sure that all excessive bacterial and debris has been removed but can also lead to delayed proliferation and extensive tissue damage resulting in formation of a chronic wound (Singh, Young et al. 2017). The purpose of the proliferation phase is to repair the defect by producing a new matrix that is needed to restore the structure and function. This phase incorporates fibroblast migration, deposition of the extracellular matrix and formation of granulation tissue (Diegelmann and Evans 2004). Epithelialization is the final stage of the proliferation phase which requires a moist environment, adequate nutrition and bacteriological control, and is modulated by several growth factors, including keratinocyte growth factor, epidermal growth factor, and basic fibroblast growth factor (Enoch and Leaper 2008). The last step of the wound healing cascade is the remodelling phase which can even take up to years depending on the wound type (Flanagan 2000). However, there would be a scar formation at the end of healing process due to several factors such as fibrotic deposition,

collagen organization and excess granulation in the case of abnormal wound healing (Rhett, Ghatnekar et al. 2008).

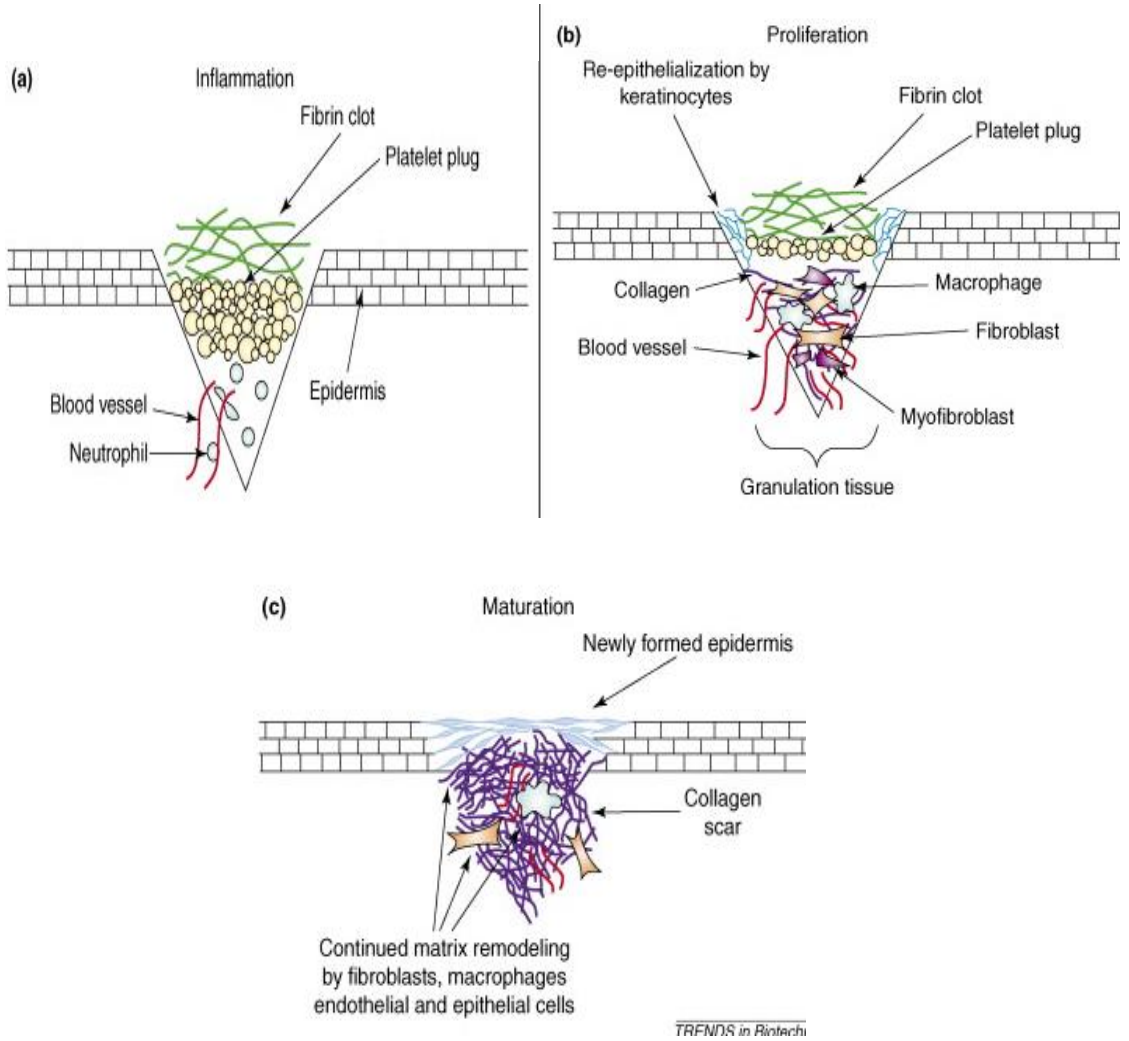


**Figure 1.2 A stereotype overview of the wound healing process which can be dived in to three overlapping phases (a) Inflammatory (b) Proliferation (c) Maturation.(Rhett, Ghatnekar et al. 2008)**

## 1.3. Wound treatments

Inhibition of healing or prolonged healing may result from various problematic conditions associated with the natural healing process. In such cases it is important to enhance the healing process by therapeutic treatments, wound dressings, tissue engineering and/or bioactive molecules (Chandika, Ko et al. 2015). Apart from the above mentioned methods

there are some advanced wound care techniques such as skin substitutes, negative pressure wound therapy and hyperbaric oxygen; however these technologies are still under development (Han and Ceilley 2017). The following section focuses on wound dressings and skin grafts, pertaining to the presented work here in this thesis.

### 1.3.1. Wound dressings

Wound dressings have evolved over the years not only to just cover up, as the basic function by providing a protective barrier, but also to enhance the wound healing process by providing a suitable environment. The key features of an ideal wound dressing are as follows (Vowden & Vowden, 2017):

- Maintaining a moist environment.
- Absorb excess wound extrudate.
- Allowing gaseous exchange.
- Protect the wound from extraneous bacteria, trauma and contamination.
- Permitting thermal insulation.
- Non-adherent, comfortable and conforming.
- Minimize the scar formation.
- Non-toxic, non-allergic and non-sensitizing.
- Cost effective and clinically effective.

Wound dressings can be classified as passive, interactive and bioactive, as previously described by (Zahedi, Rezaeian et al. 2010). Passive dressings are traditional dressings, including cotton wool, natural or synthetic bandages, and gauzes. These types of dressings tend to become adherent thus causing discomfort, lose their protective function when they

become moist, need regular changing and provide less gaseous exchange. Interactive dressings include materials that can retain and maintain a moist environment while allowing gaseous permeability and providing a barrier against bacteria (Byrne 2014). Films, foams, hydrogels, hydrocolloids and alginate can be categorized as interactive wound dressings. Bioactive dressings are made up of biomaterials that play an active role in the wound healing process and are superior to the aforementioned dressing types. Collagen, chitosan, alginate and elastin are used in these bioactive dressings which can enhance the healing process rapidly (Doillon, Whyne et al. 1986, Paul and Sharma 2004). Their biodegradability, biocompatibility and ability to incorporate various antimicrobial agents have led to advances in bioactive dressings.

### 1.3.2. Skin grafts

Skin grafting is a surgical procedure for covering up a wound with skin, or skin substitute, with the purpose of protecting the body from fluid loss, aiding in temperature regulation, helping to prevent disease-causing bacteria or viruses from entering the body and facilitate skin repair and regeneration. Autografting is a procedure that uses the skin from another area of the patient as a permanent covering. Although this is a much preferred method, in cases like extensive injuries where donor sites are limited or depending on the patient's condition, the use of autografts could be precluded (Murphy and Evans 2012). Allografts (use of the skin from another human being) and xenografts (use of an animal's skin, mainly from pigs) can only be used as temporary coverings as they come with issues of immune rejection, and possible disease transfer. Hence, synthetic skin substitutes/tissue engineered skin grafts provide a better alternative for autografts though most of the current skin substitutes are costly. Skin substitutes consist of biomaterials of synthetic or biological origin that can be

used as a skin replacement (Shevchenko, James et al. 2009). A detailed review on available skin substitutes has been done by Shevchenko, James, & James, 2009. According to Shevchenko et al. these biomaterials should be non-toxic, immunogenic, biodegradable, exhibit similar mechanical properties of skin, able to support the reconstruction of the damaged skin and provide protection from infections. It is also a significant advantage if the substitutes are cost effective, readily available and user friendly.

## 1.4. Conventional fabrication strategies and their limitations

There are several biomaterial scaffold fabrication strategies that have been developed and explored thoroughly in the literature and these techniques can be mainly divided into conventional and advanced fabrication techniques (Zhao, Gu et al. 2018, Eltom, Zhong et al. 2019). Conventional fabrication techniques include solvent casting, particulate leaching, freeze-drying, gas foaming, phase separation. Although there are some advantages like relative simplicity and low cost, these techniques are limited to meet all major requirements for scaffolds fabrication and mass production. These include limited capacity to control precise pore size, pore geometry, pore interconnectivity, spatial distribution of pores and construction of internal channels within the scaffold (Peltola, Melchels et al. 2008). In addition, some of the conventional techniques use organic solvents that lead to cytotoxicity of scaffolds. Limitation in the material selection is also a significant problem in the above conventional techniques in developing scaffolds with suitable microenvironments for supporting cell functions. One important conventional scaffold fabrication technique is electrospinning. Electrospinning is a technique that utilizes electrical fields to dispense fibres to fabricate nanoscale scaffolds with nanofibrous architectures (Pignatello 2013). It has overcome some major drawbacks associated with other conventional techniques by having

the ability to fabricate 3-dimensional nanofibrous scaffolds, enabling improved cell binding and proliferation (Pignatello 2013). However, this technique still has limitations such as fabricating scaffolds with complex structures and dependence on many electrospinning parameters (Huang, Zhang et al. 2003). Table 1 gives a short summary of the pros and cons of conventional scaffold fabrication techniques.

**Table 1: Pros and cons of some conventional scaffold fabrication techniques. (Adapted from (Subia, Kundu et al. 2010, Eltom, Zhong et al. 2019))**

| Methods | Pros | Cons | References |
|---|---|---|---|
| Solvent casting/ Particulate leaching | Control over Porosity, pore size and crystallinity | Limited mechanical property, residual solvents and porogen material | (Xiang, Liao et al. 2006) |
| Gas foaming | Free of harsh organic solvents, control over porosity and pore size | Limited mechanical property, inadequate pore interconnectivity | (Ikada 2006) |
| Phase separation | No decrease in the activity of the molecule | Difficult to control precisely scaffold morphology | (Smith, Beck et al. 2007) |
| Freeze drying | High temperature and separate leaching step not required | Small pore size and long processing time | Boland et al., 2004;(Mandal and Kundu 2008) |
| Self-assembly | Control over porosity, pore size and fiber diameter | Expensive material, complex design parameters | (Zhang 2003) |
| Electrospinning | Control over porosity, pore size and fiber diameter | Limited mechanical property, pore size decrease with fiber thickness | (Liang, Hsiao et al. 2007) |

## 1.5. Bioprinting

Biofabrication is an interdisciplinary research branch which bridges biology, biomaterial sciences and mechatronic engineering with various potential applications in tissue engineering (Sears, Seshadri et al. 2016), disease pathogeneses, and drug pharmacokinetic studies, biochips and biosensors, cell printing, patterning and assembly, and emerging organ printing. Within biofabrication, bioprinting is a branch of an additive manufacturing technique that allows generation of complex living or non-living biological products from raw materials which are commonly known as bioinks (Mironov, Trusk et al. 2009) or biomaterial inks. Excelling over conventional fabrication techniques, bioprinting offers a better and much controlled spatial distribution to combine biomaterials, cells, and growth factors to mimic the native tissue so that the construct can promote the regeneration of healthy and vascularized tissues.

Based on their working principles, bioprinting systems can be primarily classified as: (1) laser-based, (2) inkjet-based, or (3) extrusion-based where each technique requires certain specific characteristics of the bioink in terms of rheology and curing conditions to achieve desirable products (Malda, Visser et al. 2013). A schematic of these three bioprinting systems is shown in Figure 1.3 and brief explanations are below as these are the 3 most common techniques. Apart from these three main systems, there are Stereolithography(SLA) and Digital light processing(DLP) which uses photosensitive polymers under precisely controlled lighting (Gu, Fu et al. 2019). SLA and DLP are solid freeform, nozzle-free technology but got numerous limitations such as the lack of proper biocompatible and biodegradable polymers, harmful effects from residual toxic photocuring reagents, the inability to completely remove the supporting structure and the need of excess of bioink material which makes these techniques not user friendly.

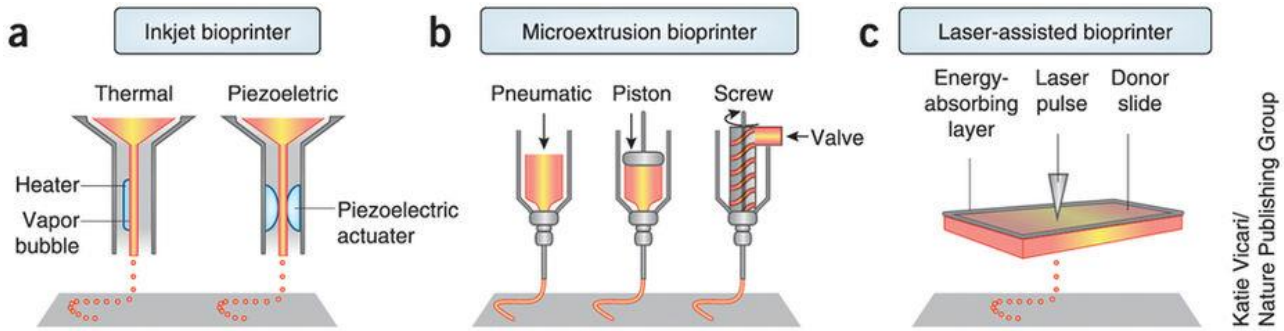


**Figure 1.3 Three main bioprinting systems (Murphy and Atala 2014).**

### 1.5.1. Laser assisted bioprinting/ Laser induced forward Transfer

Laser assisted bioprinting technique (LAB) is based on the principles of laser-induced forward transfer and typically consists of a pulsed laser beam, focusing system, "ribbon" (glass covered with a laser energy absorbing layer) and layer of biological material (Murphy and Atala 2014). The focused laser pulses cause local evaporation of the absorbing layer to generate a high gas pressure that drives the ink compound towards the collector slide (Malda, Visser et al. 2013). This technique is less common due to several drawbacks including the high cost and requirement of rapid gelation kinetics. However, it holds some special advantages such as the possibility to work with a range of viscosities, being free of clogging issues since it is a nozzle free approach, and not causing mechanical stress to the cells, as it is a non-contact printing method (Guillotin and Guillemot 2011). Guillotin et al. have demonstrated that the LAB is capable of printing versatile biological patterns with high printing speeds, high cell density and single cell level resolution (Guillotin, Souquet et al. 2010).

### 1.5.2. Inkjet printing

Inkjet printing, similar to all the other bioprinting techniques, uses a bioink (usually a hydrogel with encapsulated cells) stored in a cartridge and generates constructs layer-by-layer by

ejecting bioink ink as droplets (Boland, Xu et al. 2006). This technique is also known as "drop-on-demand" and typically uses thermal, piezoelectric or electromagnetic approaches to eject the ink droplets. Boland et al.(2006) used a thermal inkjet printer to successfully fabricate 3D cellular assemblies with high cell viability and they have also shown that many layers or porous/channels can be printed (Boland, Xu et al. 2006). Many studies have shown that inkjet bioprinting can be used as an effective tool for medical applications (Nakamura, Nishiyama et al. 2006, Cui, Boland et al. 2012), especially because of the small droplet volumes that enable high printing resolution that can produce natural tissue architectures of similar length scale. The main drawbacks of this technique are the requirements placed on the material. The typical nozzle size is in the range of 20–30 μm which limits the viscosity of the material used as the bioink below 20 mPa $s^{-1}$ (Jungst, Smolan et al. 2015). The droplets should polymerise or stabilize quickly before the addition of subsequent droplets (Skardal and Atala 2015) which makes the inkjet printing highly dependent of the droplet solidification.

### 1.5.3. Extrusion printing

In extrusion printing, desired structures are generated by dispensing a continuous strand of ink material with or without living cells. The process is driven by mechanical or pneumatic forces. Among the three bioprinting techniques extrusion printing is the most widely used technique due to its affordability, ability to construct structures with higher cell density, ability to use multiple ink materials with multiple printing heads, higher printing speed and compatibility with a wide range of fluid properties (You, Eames et al. 2017). Materials with shear thinning property are more suitable for this scenario so that the solution can maintain a low viscosity when passing through the nozzle. Upon deposition, a rapid recovery of the ink viscosity is required to maintain the shape fidelity. The main drawback of this method is shear induced cell damage during the printing process which have a cell survival rates in the range of 40–86%,

with the rate decreasing with increasing extrusion pressure and increasing nozzle gauge (Murphy and Atala 2014). This can be addressed by ink formulations to minimize the shear stress that cells may experience during printing. Extrusion printing has shown promising results in many basic research fields including tissue engineering and regeneration medicine (Ning and Chen 2017, You, Eames et al. 2017), and drug screening (Snyder, Hamid et al. 2011).

## 1.6.Biomaterial inks and their printability for extrusion-based printing

A biomaterial ink is considered as a key component in bioprinting. First and foremost, it is vital to understand the difference between a bioink and a biomaterial ink as the terms are being used divergently in the literature. Groll, Burdick et al. have provided a sophisticated explanation of the evolution of the two terms with the general definition and identifying the distinction (Groll, Burdick et al. 2018). Accordingly, "an aqueous formulation of polymers or hydrogel precursors that contain biological factors would be considered biomaterial inks, that—by definition—would become bioinks following the addition of cells into that formulation". Here in this study, the inks developed do not involve cells while printing, so they are termed as "biomaterial inks".

An ideal biomaterial ink should satisfy two main objectives; first the biological requirement of the application, and secondly the mechanical and physical requirement of the printing technique (Chung, Naficy et al. 2013). Since this particular work aims to develop extrusion-based biomaterial ink for wound healing application, a detailed discussion on extrusion-based biomaterial ink is given below.

In extrusion printing, as described in Section 1.5.3, a continuous strand of biomaterial ink is being extruded through a nozzle in a pre-defined pattern. So it is desirable to maintain a low viscosity during the extrusion to avoid shear stress that would ultimately lead to gel fracture, and to avoid potential jamming (Chimene, Lennox et al. 2016). To elaborate more (Figure 1.4),

once the applied pressure exceeds the yield stress, material starts flowing through the nozzle. Due to the shear stress, the network of polymer chains reorganizes in a manner which reduces the viscosity (shear thinning) thus facilitating the flow through the nozzle to produce a continuous filament to deposit in a desired manner. Such behaviour is shown in thixotropic materials as its apparent viscosity decreases with time under a constant shear rate (Li, Liu et al. 2016). Shape fidelity of the printed filament depends on how fast the material can reinstate the network after removal of the shear stress until the post-curing process. Due to this purpose, many researchers are interested in integrating shear thinning behaviour or thixotropic behaviour and self-recovery ability when developing a biomaterial ink to be used in extrusion printing (Guvendiren, Lu et al. 2012).So as a summary, rheological parameters including viscosity, shear thinning property, yield stress and self-recovery ability should be considered when establishing a biomaterial ink for extrusion based printing (Malda, Visser et al. 2013). Furthermore, it is highly recommended to apply a post-curing method to improve the mechanical integrity of the printed structure (Highley, Rodell et al. 2015).

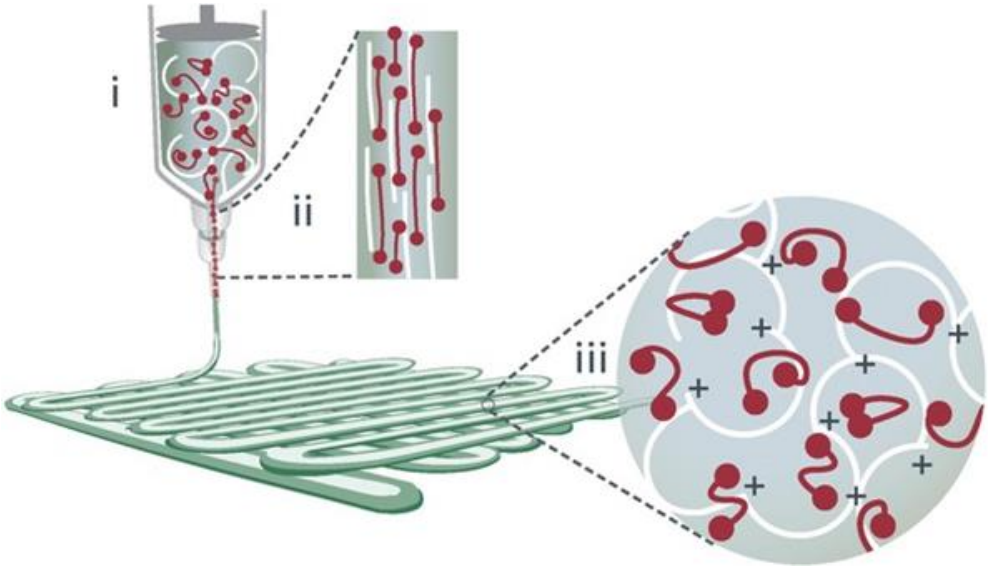


**Figure 1.4 Schematic representation of shear thinning behaviour and self-recovery of a biomaterial ink. (Adapted from Malda, Visser et al.)**

From a biological aspect, a biomaterial ink should be biocompatible. It should not only be non-toxic to the cells but also provide the environment for the cells to proliferate and function (Gopinathan and Noh 2018). It is desirable for the biomaterial ink to be biodegradable, as well as have biological functional properties specific to the targeted application. For example, in the wound healing application, a biomaterial ink with both antibacterial properties and the ability to stimulate the wound healing process would be desirable. Moreover, Chimene et al. have described some design parameters for development of biomaterial inks (Chimene, Lennox et al. 2016). A first approach is to incorporate biopolymers that contain cell attachment molecules and facilitate cell-matrix interactions, including adhesion, migration, proliferation and differentiation, thus helping matrix remodelling and extracellular matrix synthesis (Ning and Chen 2017). Incorporate therapeutic drugs and use of nanomaterials is highly considered as a new approach in controlling the release kinetics of the biomolecules to increase the therapeutic efficiency.

### 1.6.1. Aqueous based biomaterial inks

Aqueous-based biomaterial inks are intensively explored for extrusion printing due to their hydrophilicity, biocompatibility and close resemblance to native tissues. They are hydrogel precursors. Following 3D printing, a rapid chemical or physical crosslinking method is required to produce and stabilise the 3D printed structure in a hydrogel form which has a polymeric 3D network that possesses high water content that permits diffusion and attachment of cells or different molecules (Chirani, Gritsch et al. 2015). Depending on their origin, hydrogels can be classified into two categories: naturally derived hydrogels and synthetic hydrogels. Natural hydrogels have inherent biocompatibility as they are components of extracellular matrix (collagen, fibrin, hyaluronic acid) or derived from natural sources (chitosan, alginate, ulvan). Due to the variation of the source, reproducibility can be compromised (Malda, Visser et al.

2013). On the other hand, synthetic hydrogels like polyethylene glycol and polyvinyl alcohol can have a high shape fidelity, as well as high reproducibility, though often result in poor biocompatibility (Tibbitt and Anseth 2009).

Hydrogels typically absorb up to thousand times of their dry weight. The first water molecules entering the dry matrix of a hydrogel will interact with hydrophilic groups in the chains, resulting in swelling of the network and exposing hydrophobic groups. The water molecules will then interact with hydrophobic groups, with all water binding to the chains defined as "bound water". After the interaction with bound water, the network will imbibe more water molecules into the space in between chains, known as "free water", due to the osmotic driving force (Chirani, Gritsch et al. 2015). This additional swelling of the network will be opposed by the crosslinking network of the hydrogel so it will reach to an equilibrium swelling level (Hoffman 2012).

The structural integrity of a hydrogel depends on its type of crosslinking network. Reversible or physical hydrogels only have a crosslinking network made up from physical interactions such as ionic, H-bonding, hydrophobic forces or molecular entanglements. Physical cross-linked hydrogels can be weak in mechanical strength. In contrast, chemically cross-linked hydrogels have a covalent crosslinking network often proving to have better mechanical stability. In bioprinting, the idea of having both physical and chemically cross-linked hydrogels is appealing, as a physical crosslinked network can better support printability while a chemically crosslinked network can be used as a post-curing method to ensure the structural fidelity of the printed shape. There are several parameters that modify the mechanical properties of a hydrogel, including crosslinking density, monomer concentration, monomer molecular weight, or via the addition of fillers and biodegradable fibres (Fedorovich, Alblas et al. 2007).

## 1.7. Material Consideration

### 1.7.1. Chitosan

Chitosan is a polycation comprising randomly distributed N-acetylglucosamine and glucosamine units linked by β (1–4) glycosidic bonds. It is a deacetylate derivative of chitin (Figure 1.5), a natural polysaccharide found in arthropods, cephalopods and some fungi (Montembault, Viton et al. 2005, Rinaudo 2006). Generally the degree of acetylation is less than 60% in chitosan, which is soluble in dilute acidic aqueous solutions (Montembault, Viton et al. 2005).

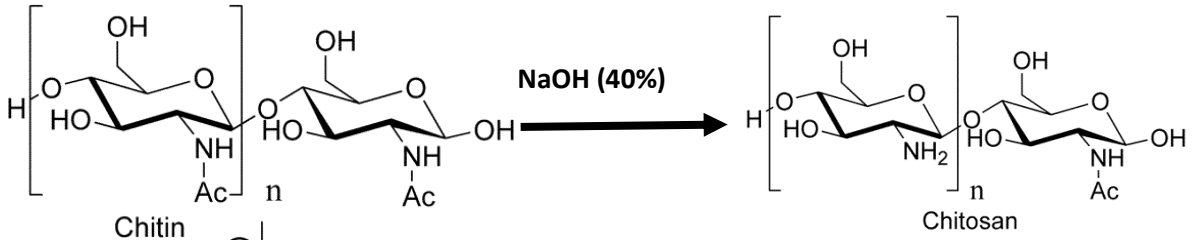


**Figure 1.5 Preparation of chitosan from chitin source : (Rabea, Badawy et al. 2003)**

Chitosan is especially of interest in wound healing applications due to its biocompatibility, biodegradability, antimicrobial activity, fungistatic properties, and ability to stimulate the healing process. Chitosan has also been intensively explored for drug delivery applications (Rabea, Badawy et al. 2003, Kumar, Muzzarelli et al. 2004, Naficy, Razal et al. 2009, Tran, Duri et al. 2013).These properties of chitosan are actively involved in all three phases in wound healing (Kumar, Muzzarelli et al. 2004, Harkins, Duri et al. 2014). Chitosan can influence platelets to stop haemorrhage in the haemostasis phase and also maintain a moist environment to maintain the cellular and tissue viability in haemostasis, inflammatory and proliferation phases.

Chitosan has demonstrated excellent antimicrobial effects in the inflammatory phase and chitosan can enhance the connective tissue matrix growth in the proliferation phase which are common delayed phases in chronic wounds (Rabea, Badawy et al. 2003, Harkins, Duri et al. 2014). Studies have shown that chitosan enhances vascularization, and a continuous supply of chitooligomers to the wound stimulates correct deposition, assembly, and orientation of collagen fibrils and assists in the reconstruction of extracellular matrix components which ultimately improve healing with minimum scar formation (Kumar, Muzzarelli et al. 2004, Naficy, Razal et al. 2009).

Major shortcomings of chitosan that limit its applications, including in the bioprinting field are: slow gelation time, poor solubility and poor mechanical properties (Yan, Davoodi et al. 2018). Therefore, modifications of chitosan have been done to overcome these limitations. Such two main modifications are:

1) Addition of small functional groups like alkyl, carboxymethyl groups etc into the chitosan chain via two main reactive groups: free amine group and hydroxyl groups in order to increase the solubility (Alves and Mano 2008).

2) Blending with other hydrogels and used as composites to eliminate the poor mechanical properties (Ozbolat and Hospodiuk 2016).

Introduction of methacrylate moieties onto chitosan chains has been explored recently to afford a water-soluble chitosan derivative with photo-crosslinkable properties (Hu, Hou et al. 2012, Diolosà, Donati et al. 2014, Zhu and Bratlie 2018). According to Zhu and Bratlie et al, methacrylated chitosan hydrogels have the potential to accelerate wound healing by responding to specific pH dependence wound healing stages (Zhu and Bratlie 2018).

Although the mechanical properties of chitosan also can be increased by chemical modifications, it involves harmful chemicals or man-made polymers to strengthen its structure

(Harkins, Duri et al. 2014). So as a "green" way, blending with naturally abundant polymers such as cellulose has been considered. HPS, Saurabh et al. have reviewed chitosan-cellulose blends and their applications (HPS, Saurabh et al. 2016). In the above review, chitosan-cellulose blend materials have been identified as materials with antibacterial properties and have been used in wound healing applications (Abou-Zeid, Waly et al. 2011, Tran, Duri et al. 2013).

Having considered all the above favourable factors, methacrylated chitosan was selected as a precursor along with a cellulose derivative (methyl cellulose) to develop the biomaterial ink in this study. However, there has only been a handful studies done on bioprinting with chitosan so far. A detailed discussion on previous studies of chitosan in the bioprinting field is given in Section 1.7.2 below.

### 1.7.2. Previous studies on chitosan in the bioprinting field

There have been a few attempts to 3D print chitosan itself but all the attempts involve use of either acidic conditions or organic solvents. Wu, Therriault et al. have used highly acidic conditions (40% v/v acetic acid, 20% v/v lactic acid and 3% v/v citric acid) to achieve high chitosan concentration and 3D printed the scaffold via solvent evaporation (Wu, Therriault et al. 2018). Ye, Felimban et al. have dissolved chitosan in 2% v/v acetic acid and extrusion printed with the use of an isopropyl alcohol bath (Ye, Felimban et al. 2014). There also have been a few studies to print chitosan with the addition of other components to enhance the mechanical properties as well as to achieve specific biological properties. $TiO_2$-supported chitosan scaffolds were developed in a previous study aiming for the photocatalytic degradation of antibiotic pollutants in wastewater (Bergamonti, Bergonzi et al. 2019). Silk particles were used as a filler to improve the printability of chitosan and have attained 3D printed scaffolds with reinforced compressive modulus and no cytotoxicity (Zhang, Allardyce

et al. 2019). In both of the above studies, since chitosan is water insoluble, an acetic acid media was used to dissolve the chitosan and the scaffolds were printed onto a coagulant medium to stabilise the structure as well as neutralize the acidic medium. A water-soluble form of chitosan has also been used in 3D printing in very few previous studies. Kufelt, El-Tamer et al. have developed a water soluble and photocurable chitosan deravative by N-succinylation modification followed by the incorporation of photosensitive methacrylate groups. The latest study on water-soluble chitosan derivative used in 3D printing would be methacrylated chitosan, named as ChiMA, developed by Sayyar, Gambhir et al. In this study, ChiMA, a water soluble and photocurable form of chitosan, was used with graphene as a filler and was 3D printed in a precipitation bath of isopropanol. Although it uses a simple modification on chitosan, the use of organic solvent can limit applications. So thoughout the litrature, chitosan 3D printing has involved acidic conditions, organic solvents or complex muti-step modifications.

So this thesis study will be focussing on the gap: that is, to develop aqueous based chitosan ink via a simple modification process which imparts water solubility and the ability to be photocured, thus removing the need to use harsh chemical environments.

### 1.7.3. Methyl cellulose

Cellulose is the most abundant biopolymer found in nature, including plants, marine animals, algae and even in amoeba (O'sullivan 1997). It is a linear homopolymer of D-glucopyranose units with β-1-4 glycosidic linkages. Cellulose consists of crystalline domains and disordered domains. The hydrogen bond interactions in the crystalline domain are very strong which makes that region less susceptible to any reactions while the less ordered region is available for hydrogen bonding with other molecules. Because of the crystalline region, the cellulose structure is insoluble in water. But the less ordered region is accessible for hydrogen bonding;

it has the water retention ability (Hubbe, Rojas et al. 2008, Habibi, Lucia et al. 2010, Kalia, Dufresne et al. 2011). Methyl cellulose (MC) is a water-soluble derivative of cellulose made from the hydrophobic substitution by methyl groups (Figure 1.6). When a certain fraction of hydroxyl groups are substituted by hydrophobic methyl groups, some intermolecular hydrogen bonds prevail which makes it water soluble (Li, Thangamathesvaran et al. 2001). Methyl cellulose is a viscosity enhancing polymer widely used as a thickener in pharmaceutical, cosmetic and food industries. Methyl cellulose also exhibits a thermo-reversible sol-gel transition which expands its application as a hydrogel in the biofabrication field. The gelation of the methyl cellulose solution occurs due to the intermolecular hydrophobic interactions, which is a function of temperature (Li, Thangamathesvaran et al. 2001). With an increase in temperature, polymer-polymer interaction becomes dominant compared with water-polymer interaction , resulting in a gel (Altomare, Cochis et al. 2016).

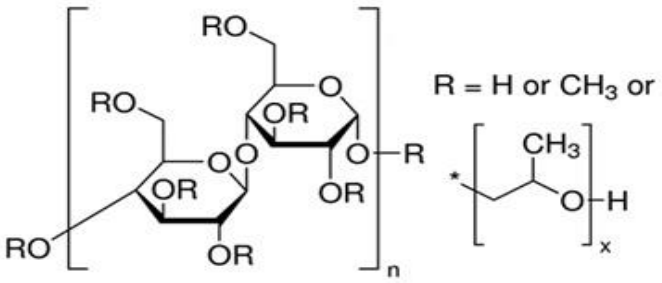


**Figure 1.6 Chemical structure of methyl cellulose.**

Methyl cellulose hydrogels are used in the 3D printing process by itself (Negrini, Bonetti et al. 2018) or blended with other polymers such as alginate (Schütz, Placht et al. 2017), hyaluronic acid (Law, Doney et al. 2018) to enhance the printing process.

## 1.8. Aims.

The main aims of this research are to develop a biomaterial ink using chitosan for the development of bioprinting in wound healing, as well as support researchers to accelerate the development of raw materials into printable inks by identifying the effective set of flow of experiments.

The aims of this study can be divided into 3 main objectives:

1) Development of water soluble and photocurable form of chitosan and formulate a range of potential biomaterial inks.
2) Determination of the printable ChiMA/MC biomaterial ink formulations with suitable physicochemical properties. This is achieved by:
    - Setting up a set of screening tests to identify the printable formulations. Identification of the physicochemical properties of the final hydrogel towards wound healing application.
    - Further investigations on the printability of selected ink formulations through rheological behaviour studies.
3) Optimization of the inks for extrusion printing. This involves:
    - Adapting a theoretical model to narrow down the printing conditions.
    - Evaluation of the printing and check the reproduction of complex geometries.
    - Explore the preliminary cytocompatibility of the printed scaffolds as a prerequisite to be used in wound healing applications.

# 2.MATERIALS AND METHODS

## 2.1.Materials

Chitosan powder: medium molecular weight – 190k-310kDa, methacrylic anhydride, methyl cellulose (4,000 cP, methoxy substitution between 27.5- 31.5%z0) and sodium hydroxide were purchased from Sigma-Aldrich (Australia) Pty Ltd. 30% ammonia solution was obtained from Chem-Supply. All the chemicals used were of analytical grade category.

## 2.2.Chitosan Functionalization

### 2.2.1.Synthesis of ChiMA (Methacryloyl chitosan)

Chitosan was modified with methacrylic anhydride to obtain a water soluble and photocurable form of chitosan. The methacryloyl chitosan was produced by following a procedure reported by Sayyar et al but with a lower amount of methacrylic anhydride (Sayyar, Gambhir et al. 2017). Briefly, 1 g of chitosan was dissolved in 80 ml of aqueous 4% acetic acid solution (1.050 g/ml) overnight to give an approximately 1.2 wt.% chitosan content followed by centrifugation to remove any undissolved particles. 2.4 g of methacrylic anhydride solution was added dropwise while maintaining the temperature of the mixture at 60 $^{0}$C and continued stirring overnight at 60 $^{0}$C. After cooling down the temperature to room temperature, the pH of the mixture was adjusted to 6.0 ± 0.2 using 30% ammonia solution. The mixture was then dialyzed (MWCO 12-14 kDa, cellulose membrane) against deionized water for 4 days and then freeze-dried (Martin Christ, ALPHA 2-4 LD plus, Germany) to obtain a white spongy material. Throughout the production and during the dialysis, the reaction vessel was covered with an aluminium foil in order to minimize light exposure. Furthermore, the dried sample was stored at -20 $^{0}$C prior to any experiments.

### 2.2.2. Characterization of ChiMA

To confirm the changes in the polymer structure after methacryloylation, proton NMR was carried out and compared to unmodified chitosan. The system used was a Bruker's Ascend 400-MHz NMR spectrometer and data analysis done with the Bruker topspin 3.7 software. A dilute solution (1-2 mg/mL) of chitosan and ChiMA was prepared in 4% deuterated aqueous acid, $CD_3COOD/D_2O$. $^1H$ NMR spectra were recorded between 0 and 10 ppm at room temperature under water suppression to avoid the solvent peak.

Secondly, Fourier transform infrared (FTIR) spectra were obtained between 400 and 4000 $cm^{-1}$ using a Shimadzu IRPrestige-21 infrared spectrometer. The spectra of ChiMA and chitosan powder were obtained with a diamond attenuated total reflectance (ATR) accessory. Atmospheric correction was applied in the Shimadzu IR solution software when processing the data to eliminate the moisture and carbon dioxide peak along with the ATR correction, smoothing and base line correction for further improvements.

## 2.3. Formulation of ChiMA-based inks using MC as a rheological modifier

ChiMA/MC biomaterial inks were prepared as below. A range of different ratios of ChiMA and MC were taken into vials. Dissolving methyl cellulose into water requires following certain steps according to the product information sheet supplied by Sigma Aldrich. 1/3 of the final required volume of water was heated up to 80 $^0C$ and was added to the ChiMA/MC mixtures with agitation using a laboratory vortex mixture (JWA- Jencons Julabo Miximatic). The mixtures were further agitated until the particles were thoroughly wetted and evenly dispersed. For the complete solubilization, the remainder of the water was added as cold water and these solutions were then cooled to 0-5 $^0C$ for another 30 minutes. Once the dispersion reached the temperature at which the methyl cellulose product became water soluble, the powder began to

hydrate, and the viscosity increased. The ChiMA/MC mixtures were again vortexed at the highest speed (3200 rpm) for at least 5 minutes at room temperature and kept overnight in a 37 $^0$C water bath for the further dissolution of ChiMA. This resulted in a clear and viscous solution/hydrogel to be used as an ink. Prior to printing, 0.1% (W/V) lithium phenyl-2,4,6-trimethylbenzoylphosphinate (LAP) photo initiator was added followed by thorough mixing and the polymer solution was then transferred directly into a printer cartridge. In order to remove air bubbles, the cartridges were centrifuged for 1 minute at 2500 rpm. The ChiMA/MC inks with the photo-initiator were subjected to three types of pre-screening tests; including initial screening test by extrudability, physicochemical characterization of their crosslinked hydrogel form and finally by semi-quantification assessment.

## 2.4.Pre-Screening of ChiMA/MC inks.

### 2.4.1.Initial screening by extrudability

Initial screening test was done in order to identify appropriate ranges of ink composition and concentration with the ability to form filaments. Manual extrusion tests were done by loading a ChiMA/MC ink into a syringe and assess if it can be continuously extruded through a printing needle of 200 µm diameter. If the material could be continuously extruded without over gelation and with minimum spreading, it was deemed extrudable and was selected for further study.

Then the basic physicochemical properties of the hydrogels made from selected ink formulations were assessed to identify expected properties of the final printed structure such as mechanical properties, water absorption, free polymer loss.

## 2.4.2.Secondary screening of the selected ink formulation via physicochemical characterisation of the crosslinked hydrogel form

Physicochemical characterisation of the crosslinked forms of the above selected ink formulations were undertaken to examine the effects of ink composition and concentration. This is to ensure that the selection of ink formulation enables

structures to be fabricated with physicochemical properties appropriate to the wound healing applications.

Uniform cast disks were prepared for each formulated ink by using a customized cylindrical mould with 8 mm inner diameter and 3 mm height. After dissolving ChiMA/MC in different desired ratios, 0.1% (w/v) LAP photo-initiator was added followed by thorough mixing using a laboratory vortex mixer at the highest speed (3200 rpm) for at least 1 minute at room temperature. These samples were centrifuged for 2 min at 3000 rpm to remove air bubbles and then injected into the mould with the use of a syringe. Finally, all samples were exposed to UV light using a Lumen Dynamic Omnicure LX400+ (400 nm light source) at a 30% intensity for 60 seconds. After crosslinking, disks were carefully removed and soaked in distilled water for 4 days for all experiments except for the free polymer loss experiment in Section 2.4.2.3.

### 2.4.2.1. Mechanical testing

Mechanical strength of the final hydrogel is vital when selecting a hydrogel for a specific application. Hence, a stress-strain curve was obtained by using a Shimadzu EZ mechanical tester with a 10 N load cell controlled by the TRAPEZIUMX software for each hydrogel to determine Young's modulus. The compression speed was set at a constant rate of 1 mm/min. Compressive Young's modulus was calculated in accordance with Equation 1 by calculating the gradient of the initial linear range of the stress-strain curve:

**Equation 1**

$$E = \frac{F/A}{\Delta L/L_0}$$

which obeys Hooke's Law, where *E* (Pa) is the Young's modulus, *F* (N) is the applied compression force, *A* ($m^2$) is the area of the cross-section perpendicular to the applied force (here it is the disk that is in contact with the upper compression plate), $L_0$ (m) original height of the disk and $\Delta L$ (m) is the displacement of the disk. For each experiment $\Delta L/L0$ was set up to 15%.

### 2.4.2.2. Water uptake capacity.

The amount of water that can be absorbed and retained within a hydrogel is an important parameter, especially for wound healing applications. Cast disks were prepared with formulated inks and all the samples were freeze-dried prior to the water uptake study and weighed to obtain their initial weights. These freeze-dried samples were rehydrated in distilled water and the equilibrium water uptake was determined by the increase in weight after carefully removing the excess surface water with a tissue paper. The water uptake capacity was determined by use of Equation 2:

**Equation 2**

$$WU\% = \frac{W_s - W_d}{W_d} \times 100$$

where $W_s$ and $W_d$ are weights of the hydrogel disks in mg when it is swollen and initial freeze-dried state, respectively.

### 2.4.2.3. Free polymer loss

In order to study the fate of un-crosslinked polymer chains within the hydrogel, a free polymer

loss experiment was carried out. In these experiments, the cast disks of ChiMA/MC were freeze-dried (Martin Christ, ALPHA 2-4 LD plus) connected to a vacuum pump operating at 0.09 mbar immediately after crosslinking and then weighed. Typically, samples freeze dried within an overnight period. The disks were then immersed in distilled water for 4 days, changing the distilled water twice daily. Immersion of the cast disks in distilled water tends to wash out the un-crosslinked polymer thus expect a decrease in weight. The samples were freeze-dried again, then weighed and the decrease in mass was identified as the amount of un-crosslinked polymers. The same procedure was carried out for pure ChiMA cast disks as a comparison.

### 2.4.3. Final screening by semi-quantification assessment.

After evaluating the range of physicochemical properties of the hydrogel another screening test was used to further narrow down the final printable ink formulations based on the layer stacking ability. The selected extrudable biomaterial inks were subjected to Semi-quantification assessment as described in Ouyang, Yao et al. (2016) where the Printability (*Pr*) is characterized by the following equation (3) in order to identify the layer stacking ability.

**Equation 3**

$$\mathrm{Pr} = \frac{\pi}{4} \times \frac{1}{C} = \frac{L^2}{16\,A}$$

where, *C* is circularity of an enclosed area, *L* is perimeter (m) and *A* is the enclosed area ($m^2$). To assess the printability value, simple two-layer printing was done with the use of Envision TEC 3D-Bioplotter (Germany). The structure and the infills were according to Figure 2.1. All the ink formulations were printed at room temperature with varying pressure and speed until the Pr value reached a maximum. To assess the *Pr* value for each ink, optical images

were analysed using ImageJ software to calculate the perimeter and enclosed area.

**Figure 2.1 The 3D CAD model of the structure and the infill used for semi-quantification assessment (only two layer printing was considered).**

## 2.5. Crosslinking kinetics by in-situ UV rheology.

Following the screening tests two lead ink formulations were selected for further characterisation. As the first step, crosslinking behaviour was monitored to assess the time required for the biomaterial inks to undergo crosslinking. The crosslinking kinetics was assessed by in-situ rheology time sweep using TA Instruments AR-G2 controlled-stress rheometer (New Castle, DE) with the UV attachment (400 nm light source). Samples containing 0.12 % (w/v) LAP were tested over 300 seconds. The frequency and strain were fixed at 10 Hz and 0.1%, respectively. The first 120 seconds were used for sample equilibration, before UV exposure for 120 seconds, during which the storage moduli (G') was monitored as a function of exposure time. Samples prepared based on pure ChiMA were also included for comparison.

## 2.6. Degradation studies

The cast disks of ChiMA/MC and pure ChiMA, were placed in 2 ml vials containing 0.5 mg/ml lysozyme and 0.5 mg/ml sodium azide ($NaN_3$) in phosphate buffered saline solution (PBS). Initial matrices were prepared as cast disks, soaked in distilled water for 4 days to remove any

free polymer, and then weighed after freeze-drying of the samples ($\boldsymbol{W_{t=0}}$). The vials were stored in an incubator and the medium was changed every 3 days. Three samples from each of the ink formulations were collected at fixed time intervals and thoroughly washed with distilled water to remove any PBS and lysozyme, and finally freeze-dried to get the final weight ($\boldsymbol{W_{t=t}}$). The weight loss percentage of each of the cast disks at fixed time intervals was determined from Equation 4.

**Equation 4**

$$\boldsymbol{weight\ loss\ percentage} = \frac{\boldsymbol{initial\ weight}(w_{t=0}) - \boldsymbol{final\ weight}(w_{t=t})}{\boldsymbol{initial\ weight}\ (w_{t=0})} \times \mathbf{100}$$

## 2.7. Rheological evaluation of the selected ink formulations

The rheological measurements were taken by TA Instruments AR-G2 controlled-stress rheometer (New Castle, DE) using a 12 mm stainless steel parallel plate geometry with a gap of 500 µm, fitted with a Peltier temperature-controlled stage. All tests were carried out in triplicate with correct loading and trimming to ensure the reproducibility of results. A solvent trap was used to eliminate the water evaporation during the experiment. All the samples were loaded in a liquid state.

### 2.7.1. Shear thinning behaviour and yield stress measurements.

Rotational shear viscosity measurements were taken in flow mode with continual logarithmical ramp of shear rate from 0.01 to 10000 ($s^{-1}$) versus time to examine the shear thinning behaviour. To quantify the yield stress, storage modulus (G') and loss modulus (G") were measured using logarithmical shear stress ramp ranging from 0.1 to 1000 Pa and yield stress was determined by the cross-over-point where G'= G" (Menger and Peresypkin 2003). In rheology, G'- storage modulus of a sample represents the elastic response, while G"- loss modulus represents the

viscous behaviour. Both experiments were done at 25 $^{0}$C (room temperature), 1 Hz frequency and 0.1 % strain.

### 2.7.2. Temperature sweep

Oscillatory temperature sweeps were performed from 5 °C to 40 °C with a constant heating rate of 2 °C/min, frequency 1.0 Hz and a strain of 0.1%. Samples were kept in an ice bath for 30 min prior to the experiment and loaded at 5 $^{o}$C. All tests were equilibrated at each experimental temperature point for 1 min to ensure the homogeneity and retain the shear history at the required temperature.

### 2.7.3. Self-recovery capability of the biomaterial inks: Step-strain

Recovery of the biomaterial inks was demonstrated by measuring the viscosity whilst under a sudden increase in shear rate from 0.1 $s^{-1}$ to 1000 $s^{-1}$ with time sweep. The system was maintained at 0.1 $s^{-1}$ for 2 minutes to mimic the at-rest condition prior to extrusion and then suddenly increasing the shear rate to 1000 $s^{-1}$ and maintaining for 1 minute to imitate the extrusion based bioprinting process. This was repeated 3 times to investigate the hydrogels recovery.

## 2.8. Window of Printability- A theoretical approach

The “bioprinting window” can be defined as a selection of a range which falls within the operating capabilities of the bioprinter. Here, the selection was done by calculating the average extrusion velocity and limiting the results within the operating capabilities of the bioprinter. Rheological data obtained from a shear-viscosity profile (shear thinning coefficients), variables such as nozzle dimensions and printing conditions of the 3D bioprinter are needed for the

calculation of extrusion velocity (Paxton, Smolan et al. 2017). According to the bioplotter setup used for printing of the biomaterial inks, the operating variables and their ranges are shown in Table 2.

**Table 2 Variables in the mathematical model**

| Variables | Applied values or range |
|---|---|
| **ΔP = Extrusion pressure** | **1- 5 bar** |
| **L = Needle length** | **13.4 mm** |
| **R = Needle radius** | **100, 125, 165 µm** |
| **$\bar{v}$ = Average extrusion velocity** | **1-20 mm/s** |

This approach is mainly dependent on the material's shear-viscosity profile, in particular the shear thinning behaviour. Shear thinning behaviour of the materials can be fitted to a power law as expressed in Equation 5:

**Equation 5| Power law for shear thinning behaviour**

$$\eta = K\,\gamma^{n-1}$$

where $\eta$ (Pa s) is the viscosity, $\gamma$ ($s^{-1}$) is the shear rate and $n$ and $k$ are the shear thinning coefficients. The extrusion velocity profile (V) between any point at the distance $r$ to the capillary wall (r = R) through a capillary tip is given by Equation 6, known as the Hagen-Poiseuille laminar flow equation (Snyder, Son et al. 2015).

**Equation 6| Hagen-Poiseuille laminar flow equation.**

$$V = \frac{n}{n+1}\left(\frac{\Delta P}{2LK}\right)^{\frac{1}{n}}\left(R^{\frac{n+1}{n}} - r^{\frac{n+1}{n}}\right)$$

Where L (m) is the capillary length, P (Pa) is the dispensing pressure and v is the extrusion velocity ($ms^{-1}$).

So according to Paxton, Smolan et al., an average velocity can be found by integrating the above equation across the cross-sectional area of the needle and dividing by the cross-sectional area (Equation 7).

**Equation 7|**

$$\widetilde{V} = \frac{[\int_{r=0}^{R} V \,.\, 2\pi\, r\ dr\,]}{\pi R^2} = \left(\frac{\boldsymbol{\Delta} P}{2LK}\right)^{\frac{1}{n}} \left(\frac{n}{3n+1}\right) R^{\frac{n+1}{n}}$$

During the printing process, the highest shear stress is exerted on the biomaterial ink when it is inside the nozzle. Thus, it is important to elucidate the capillary flow analysis inside the nozzle, including the shear rate and stress (to investigate the forces being experienced by the biomaterial ink) and residence time (to determine how long the forces act upon the biomaterial ink). Shear stress ($\boldsymbol{\tau}$) of a non-Newtonian fluid can be given by:

**Equation 8**

$$\boldsymbol{\tau = K\, \dot{r}^{\,n}}$$

where ṙ is the shear rate ($s^{-1}$) and K, n are shear thinning coefficients (Ouyang, Yao et al. 2016). As shear rate can be expressed by $\frac{\partial V}{\partial r}$ , Equation 9 is known as the Ostwald-de-Waele relationship for shear stress as a function of velocity gradient.

**Equation 9**

$$\boldsymbol{\tau = K \left|\frac{\partial v}{\partial r}\right|^{n}}$$

According to Suntornnond, Tan et al. shear stress in a capillary flow can be found by use of Equation 10 (Suntornnond, Tan et al. 2016):

**Equation 10**

$$\boldsymbol{\tau = \frac{\Delta P\, r}{2L}}$$

Rearranging the above equations 8, 9 and 10 yields the following equation 11 for shear rate, and by integrating it with boundary conditions r=R to r=0 gives Equation 6 for the velocity of a non-Newtonian fluid at a distance r.

**Equation 11**

$$\boldsymbol{\frac{\partial v}{\partial r} = \left[\frac{\Delta \mathrm{P} r}{2LK}\right]^{\frac{1}{n}} = \dot{\mathrm{r}}}$$

To examine the flow profile inside the needle, shear stress (Equation 10) and shear rate (Equation 11) were used assuming that each ink was being extruded using the parameters of: 100 µm inner radius R, needle length (*L*) 13.4 m and 5 bar pressure(***Δ*** P). Equation 12 defines the residence time in the needle where *L* is the capillary length and *v* is the extrusion velocity at a given distance (Equation 6). All together (Equation 6,10,11 and 12) defines the printing process in terms of extrusion velocity, stress magnitude and duration.

**Equation 12| residence time equation**

$$t = \frac{L}{v}$$

## 2.9.Extrusion printing of ChiMA/MC inks.

Extrusion printing of the lead formulated biomaterial inks was undertaken using Envision TEC 3D-Bioplotter (Germany). 3D CAD through solid works was used to create the scaffold architectures and exported as STL files to be sliced via bioplotter RP® software (Figure 2.2: A & B). The infill of the scaffold was set to continuous strands of angles $0^0$ and $90^0$ (Figure 2.2:

C) with a 1mm distance. Nordson A 27-gauge needle was used in every printing run and the cartridge temperature was set to $18^0$C for 3% ChiMA/2% MC and $25^0$C for the 2% ChiMA/3%MC respectively. Above extrusion temperatures for each ink were found experimentally. The platform temperature was kept at room temperature throughout the printing process. Once in every 4-5 layers, scaffolds were directly crosslinked with 400 nm light with 30% intensity for 30 seconds to ensure structure fidelity and finally 60 seconds to complete the crosslinking of the scaffold.

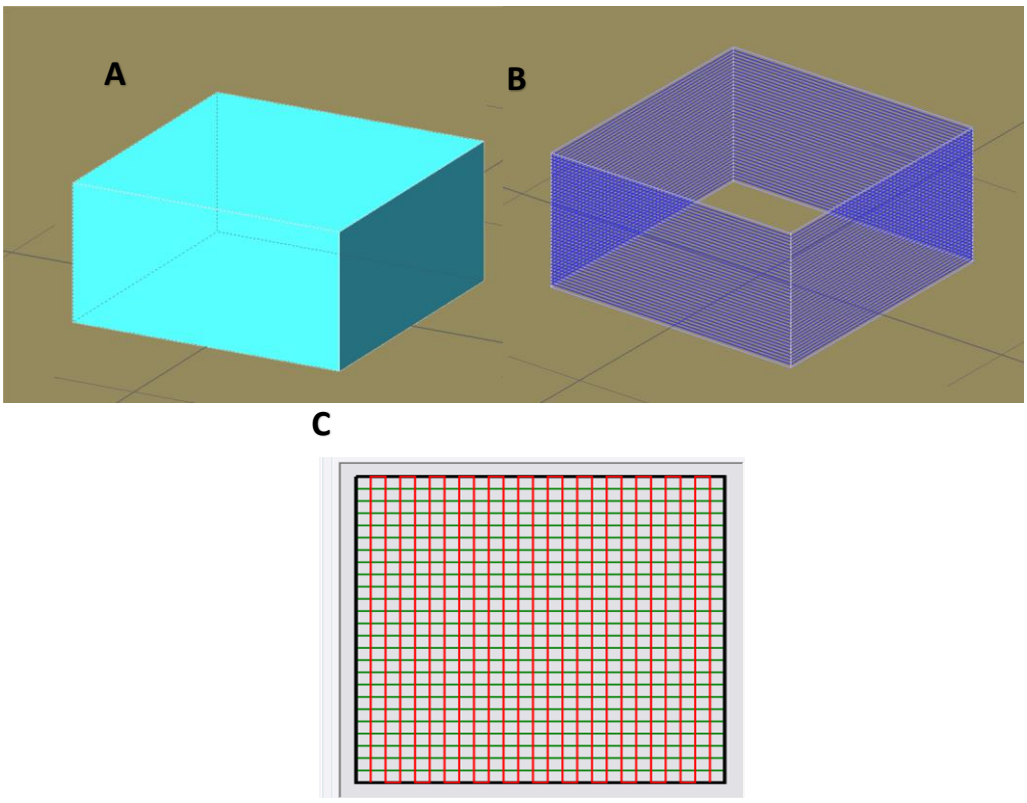


**Figure 2.2 (A) CAD design of the basic cube shape (B) Sliced version of the CAD design (C) The infill of the scaffold was set to continuous strands of angles $0^0$ and $90^0$.**

### 2.9.1. Effect of structure diameter evaluation with print speed

The strut diameter was further evaluated with the printing speed for the two biomaterial inks. A cube scaffold 10 × 10 × 2 mm with infill as shown in Figure 2.2 was used as the basic structure and two layers were printed and images were taken from the bioplotter at the end of each layer printing. Strut diameters were assessed through imageJ software. In order to

compare the two inks, both structures were printed at 5 bar pressure using an A 27-gauge needle (200 µm diameter).

### 2.9.2.Printing accuracy

In addition, the printing accuracy of the inks was evaluated in terms of the ability to correctly reproduce various CAD-designed shapes (Figure 2.3). The images taken with the built-in camera in the 3D bioplotter was qualitatively analysed to measure the correct reproducibility of the complex structures. Images were taken up to 8 layers of printing.

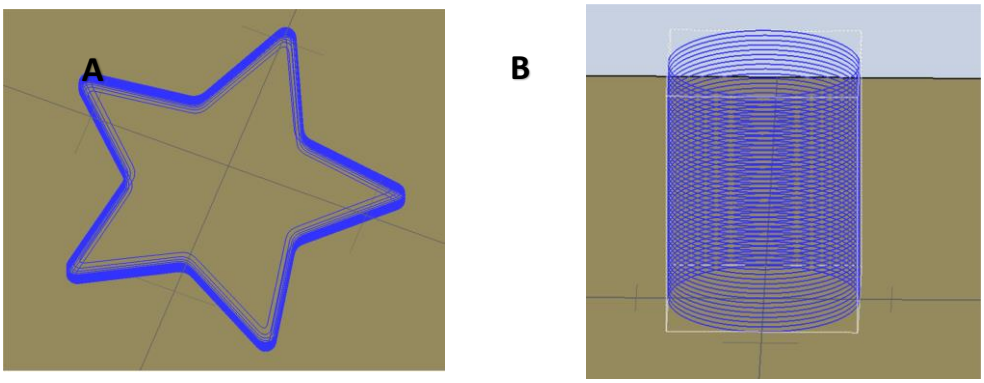


**Figure 2.3 Complex geometries designed for testing accuracy: (A) Star shape, (B) cylinder shape.**

## 2.10. Preliminary cytocompatibility of 3D printed ChiMA/MC scaffolds.

Cell-matrix adhesion and cell viability were assessed for the ChiMA/MC biomaterial. Scaffolds were printed as described in Section 2.9 and incubated for 3-4 days in distilled water, changing the media twice a day to remove any un-crosslinked polymer. Scaffolds were freeze-dried prior to the cell work and sterilized 20 min under UV light on each side.

Human dermal fibroblasts (HDFs) obtained from Cell Applications, Inc. (San Diego, CA, USA) were used at passages 8-15, as a model cell line for this study. HDFs were cultured

according to the standard procedures in high glucose Dulbecco's modified Eagle's medium (DMEM) supplemented with 10% fetal bovine serum and 1% penicillin-streptomycin in a humid incubator at 37 °C and 5% $CO_2$. When HDF reached 80% confluency, cells were passaged, resuspended and seeded at a density of $0.5 \times 10^6$ cells per scaffold. Fluorescent live/dead cell staining with calcein AM and propidium iodide (Life Technologies, Australia) respectively was used at day 1 and day 7 to determine cell viability in the 3D printed scaffolds. Briefly, the sample was incubated at 37 °C with 1:200 dilution of calcein AM to stain live cells (green colour) for 25 minutes while avoiding light. During the last 5 minutes of calcein staining, propidium iodide was used to stain the dead cells (red colour) at 1:1000 dilution. Then the cells were washed twice with PBS and the media was replaced with fresh culture media until images were acquired using laser confocal fluorescence microscopy with a Leica confocal microscope (Leica TSC SP5 II).

# 3. RESULTS AND DISCUSSION

Advances in 3D bioprinting in biomedical engineering create a challenge in developing suitable ink materials for fabrication in order to meet the demands imposed by different applications. More importantly, ink development should ultimately satisfy several criteria in terms of printability, biocompatibility, biomimetic properties of target tissues and maintaining structural as well as mechanical stability (Kim, Yeon et al. 2018). Naturally derived polymers are of interest due to their hydrophilic nature, biocompatibility and the ability to form hydrated structures simulating natural soft tissue (Silva, Reis et al. 2016). Most natural polymers however pose a problem when used as ink constituents, as they are too soft to support themselves within a fabricated structure. Chitosan is such material with many useful intrinsic properties in wound healing but with several limitations. In this study, a new biomaterial ink was developed from chitosan addressing its limitations. The approach that was used for the development of biomaterial ink is shown in Figure 3.1.

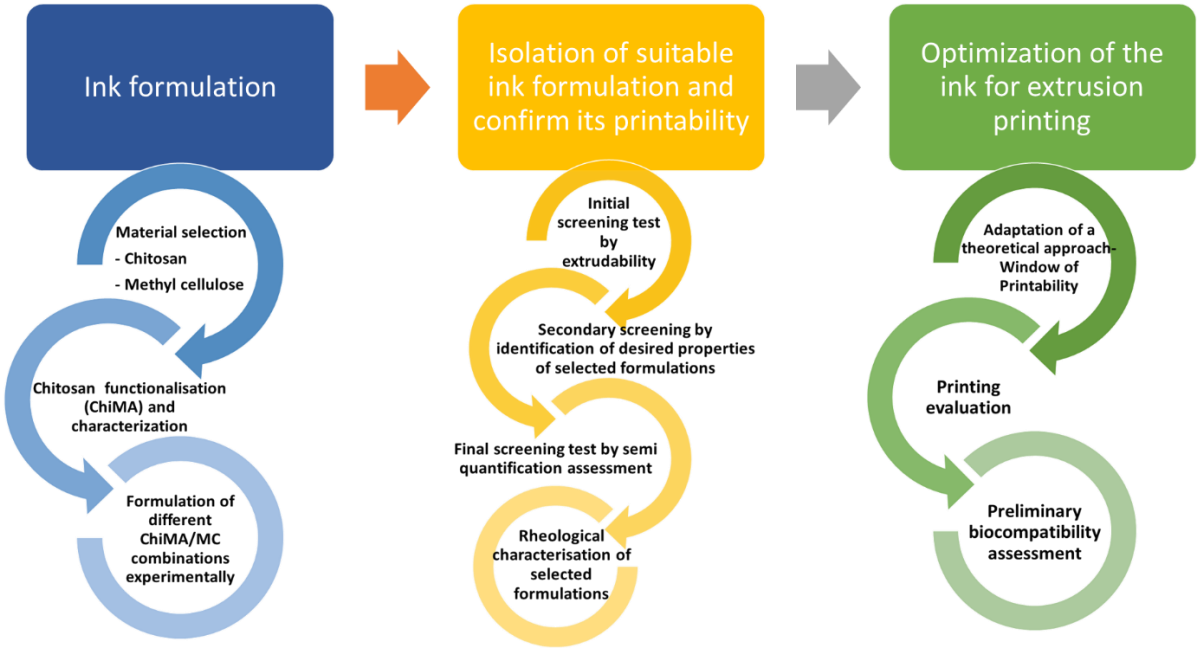


**Figure 3.1 The approach used for the development of Chitosan based biomaterial inks.**

As the first step, chitosan was functionalized with methacrylamide groups (ChiMA) to introduce water solubility and photo-crosslinkable moieties to allow post-printing crosslinking as a way of improving the stability of the 3D printed structure. A range of inks was formulated using ChiMA and methyl cellulose which is a viscosity enhancing polymer (Negrini, Bonetti et al. 2018). Identification of the optimal formulations was accomplished by investigating the key properties required for 3D printing (filament formation and layer stacking ability) along with the assessment of physicochemical properties that are expected to be imparted to the final structure as screening tests. Selected formulations were then used for further experiments, including evaluation of the rheological properties in extrusion printing.

## 3.1.Synthesis of ChiMA

Chitosan is a deacetylate derivative of chitin and it consists of repeating units of glucosamine rings (a) and N-acetylated glucosamine rings (b). These repeating units contain hydroxyl groups and amine groups that are sensitive to chemical functionalization. Here, part of the primary amine groups of chitosan repeating units (c) are modified with methacrylic anhydride and yield methacrylamide chitosan (ChiMA) which is a water soluble and photo-crosslinkable form of chitosan. The general reaction scheme of ChiMA preparation is shown in Figure 3.2. Methacrylamide chitosan was obtained with a 46% yield. Characterization of ChiMA was then undertaken to confirm the modification.

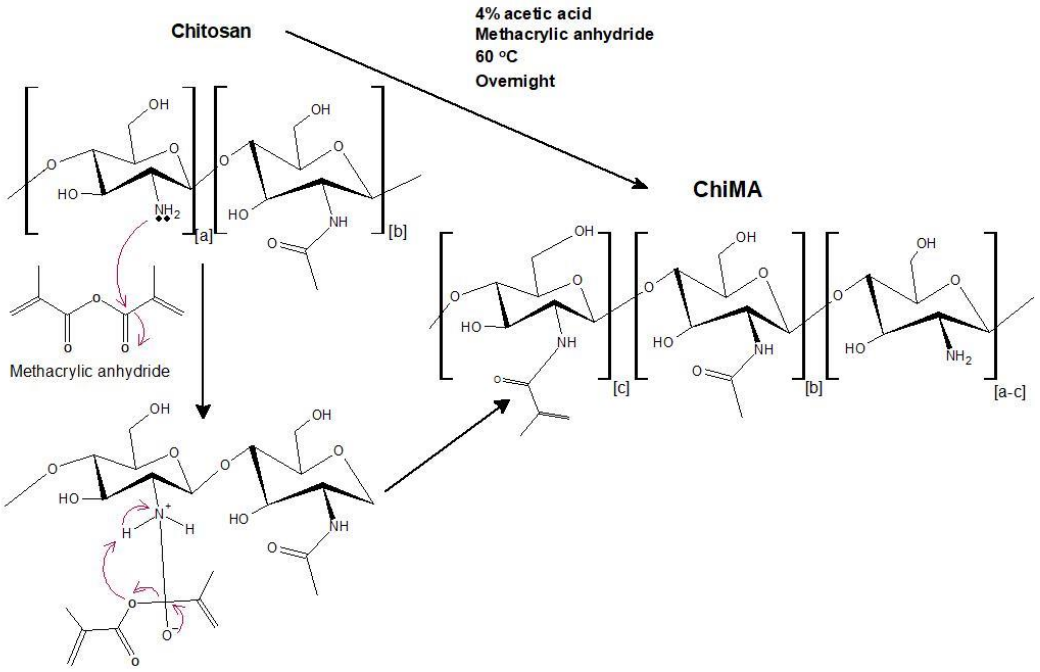


**Figure 3.2 General reaction scheme for the chitosan methacrylation.**

### 3.1.1.FTIR analysis

Samples were analysed using FTIR spectroscopy to investigate the changes in the polymer structure after the methacrylation reaction. As Shown in Figure 3.3, the strong band around 3360 $cm^{-1}$ in both spectra can be attributed to N-H stretching, O-H stretching and also due to intramolecular hydrogen bonding (Fernandes Queiroz, Melo et al. 2014). The two bands in each spectrum between 2963-2856 $cm^{-1}$ are attributed to alkyl C-H stretching and bending. The signals at 1650 and 1565 $cm^{-1}$ in the chitosan spectrum could be due to the C=O stretching and N-H bending respectively (Sayyar, Gambhir et al. 2017). Although similar peaks appear in the ChiMA spectrum with different intensities, it is difficult to make a definitive assignment since alkenyl C=C stretching also appears in the same range. The characteristic absorption peaks in the range 1030 to 1160 $cm^{-1}$ correspond to C-N stretching, C-O stretching and asymmetric stretching of C-O-C bridge. In order to get more definitive confirmation on modification further analysis was carried out with $^{1}H$ NMR spectroscopy.

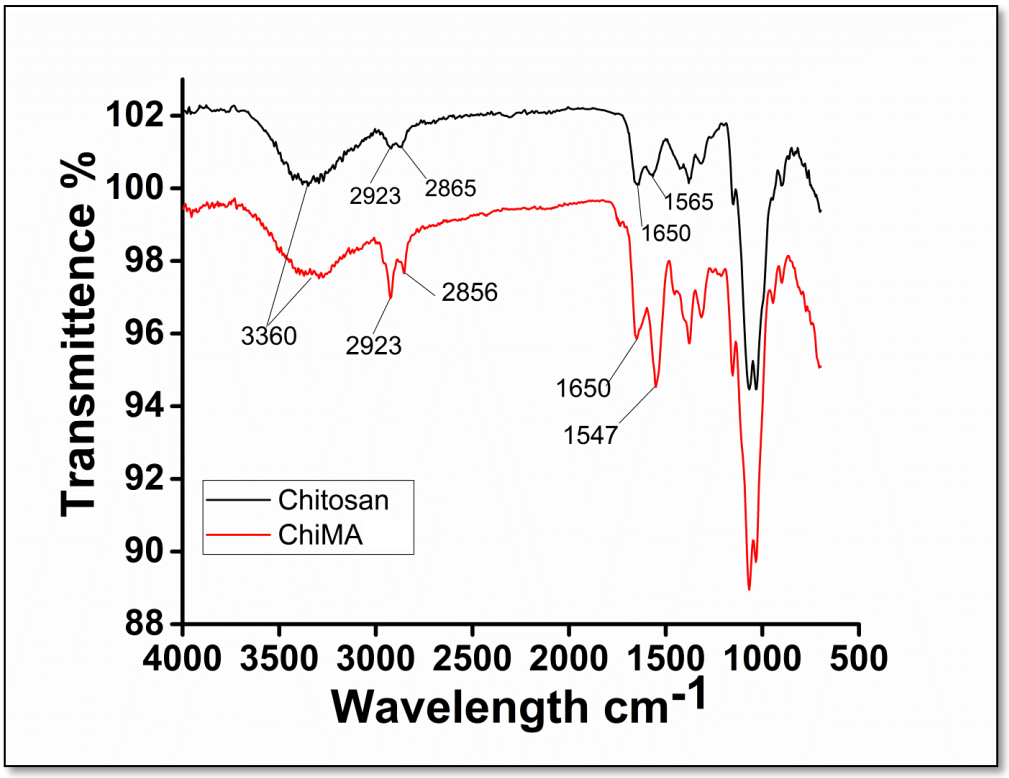


**Figure 3.3 FTIR spectra for chitosan and ChiMA.**

### 3.1.2. $^{1}$H NMR analysis

The $^{1}$H NMR spectra that are used to confirm the methacrylamide modification on chitosan are shown in Figure 3.4. The typical $^{1}$H NMR spectrum of chitosan shows the distinctive peak at 1.9 ppm, arising from the methyl groups of the acetyl moieties on chitosan. The single peak at 3.1–3.2 ppm and broad signal spectrum between 3- 3.9 ppm represent protons of glucosamine (GlcN) ring and methyl from the hydroxymethyl on the glucosamine ring respectively (Kasaai 2010). After the modification with methacrylic anhydride, ChiMA shows additional peaks at 5.5 and 5.9 ppm corresponding to the vinyl protons of the methacrylic groups which verifies the modification. Also, the additional peaks (below 1.8 ppm) in the ChiMA spectrum which partially superimpose with the signal of the methyl group of the acetyl moieties is due to the methyl group of the methacrylate moieties on the polymer chain.

The degree of modification of the polymer chain was assessed by comparing the integrated

area of the signals arising from the two vinyl protons of the methacrylated groups (5.5 and 5.9 ppm) to that of the signal arising from the six protons of the glucosamine ring (methyl from the hydroxymethyl and anomeric protons on the glucosamine ring) (Yu, Kazazian et al. 2007, Diolosà, Donati et al. 2014, Sayyar, Gambhir et al. 2017). The integral of a signal is proportional to the number of nuclei contributing to the signal, so the degree of modification was calculated according to Equation 13 (Lavertu, Xia et al. 2003, Kasaai 2010). The degree of modification was found to be 50%.

**Equation 13 Determination of the degree of modification on chitosan**

$$Degree\ of\ modification = \frac{(integral\ of\ vinyl\ protons\ at\ 5.5\ and\ 5.9\ ppm)/_2}{integral\ of\ anomeric\ protons\ of\ the\ polysaccaride\ chain/_6}$$

The degree of modification was found to be lower than that reported by Sayyar, Gambhir et al. due to a lower amount of methacrylic anhydride that was used to decrease the methacrylation to achieve water solubility of the chitosan. Although the factors determining the intrinsic properties (stimulation of wound healing , anti-bacterial effect, anti-inflammatory effect) of chitosan are largely unknown it is believed that most of the properties may depend on the concentration of the free $NH_2$ groups within the polymer (Fei Liu, Lin Guan et al. 2001, Aranaz, Mengíbar et al. 2009). For the methacrylation modification in this study, the $NH_2$ groups are consumed (Yu, Kazazian et al. 2007). Therefore a lower degree of methacrylation is favoured. The carbon-carbon double bond of the methacrylate group provides the reactive site for the photo-crosslinking. This fulfills the requirement of a precursor material for a bioink that has post-curing ability as a way of achieving structural fidelity.

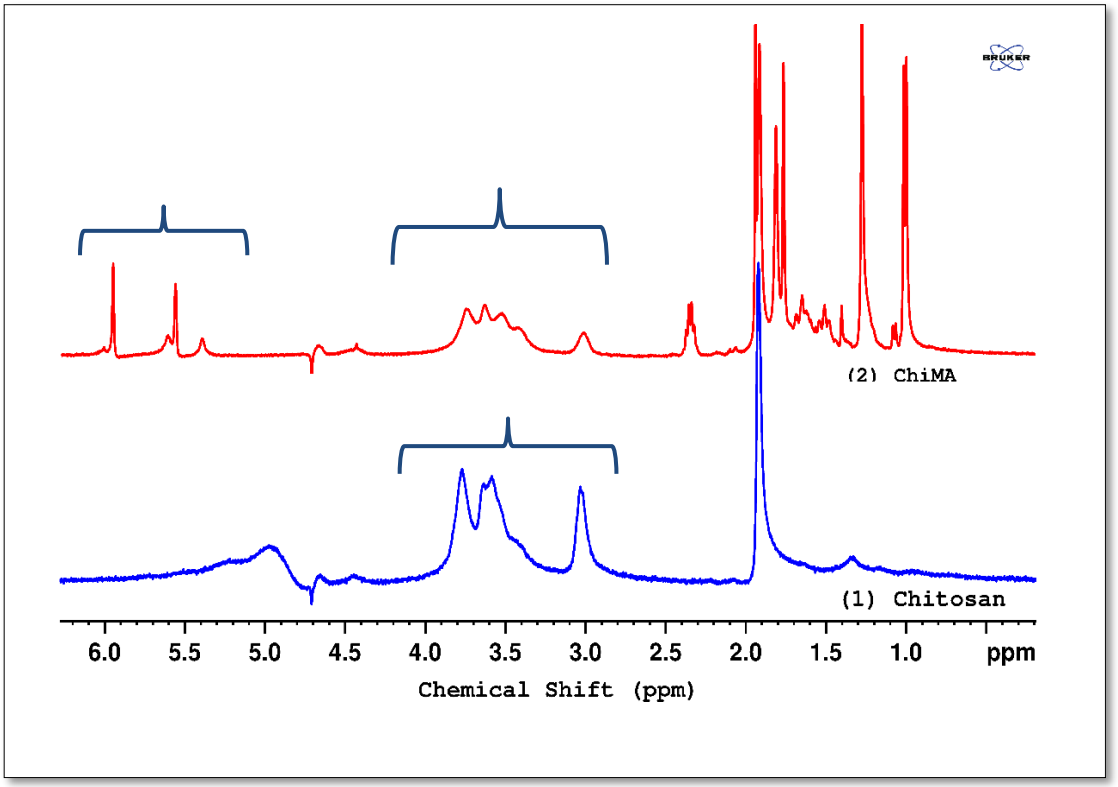


**Figure 3.4 $^{1}$H NMR spectra of chitosan (blue) and ChiMA (red) in $CD_3COOD/D_2O$ (40 mg/ml) at room temperature.**

## 3.2.Initial screening test: By extrudability.

The next step of ink development was to identify printable formulations. The maximum concentration was experimentally found to be 3% for ChiMA and 5% for methyl cellulose, above which it is difficult to achieve a homogenous solution. Inks with different combination of ChiMA and methyl cellulose within the above ranges were prepared as clear and viscous solutions.

As decribed by Chimene, Lennox et al., two fundamental requirements of extrusion-based bioinks are the ability of the material to be continuously extruded from the nozzel (extrudability) and then self-heal upon deposition to keep the integral shape of the printed structure (Chimene, Lennox et al. 2016). Initial screening test was used to determine the concentrations that satisfied one of the above requirements: the ability to form continuous

filament which is also known as extrudability. A simple manual extrusion test was performed and was able to determine the concentrations of ChiMA/MC that could form stable filaments.

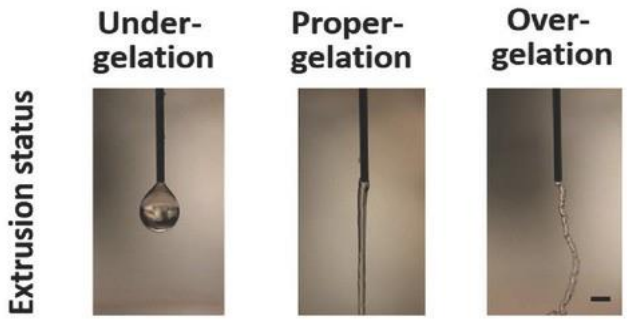


**Figure 3.5 Evaluation of extrudability of a biomaterial ink (Adapted from (Kyle, Jessop et al. 2017)**

ChiMA/MC concentrations that were too liquid resulted in an under gelation form (droplet formation), while concentrations that were too viscous resulted in over-gelation (over solidification), as shown in the extrusion status reported by Kyle, Jessop at al. (2017) under Figure 3.5. Henceforth, these concentrations were not considered. Using this method of evaluation, the omitted formulations are shown in Figure 3.6 in dark red (under-gelation) and light pink (over-gelation) colours. The formulations that demonstrated appropriate gelation behaviour are shown in Figure 3.6 in green colour.

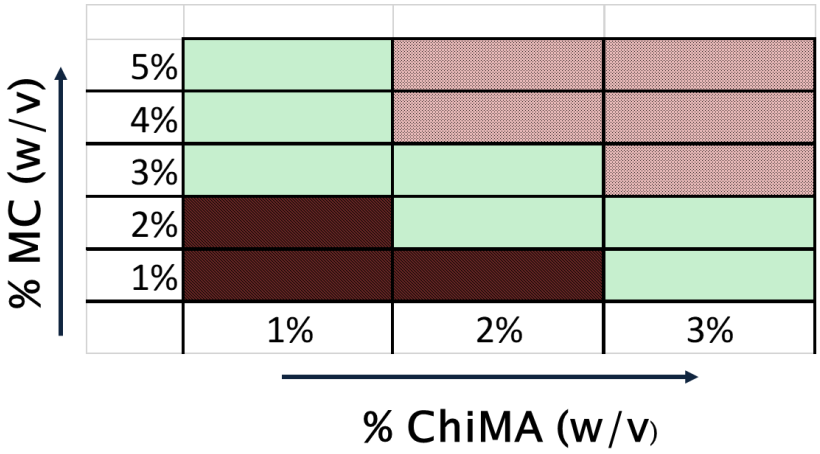


**figure 3.6 Extrudability of different ChiMA and MC concentrations. Unprintable samples are indicated in dark red and light pink colours as under-gelation (too liquid) and over-gelation (too solid) respectively.**

Six different ChiMA/MC ink formulations showed potential use as biomaterial inks in terms of ability to form continuous filaments. Using these six formulations, cast hydrogels disks were made and used to measure the physicochemical properties as a secondary screening test. This was done as a way to identify beneficial properties of the hydrogel, which would reflect upon the final structure.

## 3.3. Secondary screening of the ChiMA/MC inks- physicochemical characterisation of the crosslinked forms of the inks by UV

This was done to examine the effects of ink composition and concentration on the physicochemical properties of the final hydrogel structure. Then use this information to assess and guide further development of ink formulations if required aiming wound healing application. As detailed below the following tests were undertaken including mechanical testing, water uptake and free polymer loss. Samples were prepared as cast hydrogels disks using a customised cylindrical mould with 8 mm inner diameter and 3 mm height. All samples were exposed to UV light using a Lumen Dynamic Omnicure LX400+ (400 nm light source) at a photo-energy of 780 mJ for 1 minute.

### 3.3.1. Mechanical testing by compression.

For applications as scaffolding materials in tissue engineering, it is important to ensure the physicochemical properties of the targeted tissue are matching with the replacing material. Since the target application of this work is related to skin, which is a highly anisotropic tissue with a wide range of Young's moduli starting from 5 kPa (Kalra, Lowe et al. 2016) up to several thousand kPa, compression mechanical testing was performed to ascertain a relevant Young's modulus range.

Figure 3.7 shows the stress-strain curves obtained for the hydrogels made from the ChiMA/MC

inks. The stress-strain curves were used to quantify the Young's modulus considering the first linear range to apply in the theoretical Equation 1| Determination of the Young's modulus. The Young's modulus of a material defines the ability of a material to resist deformation against an applied external force (McKee, Last et al. 2011). The calculated Young's modulus for each hydrogel are shown in Figure 3.8.

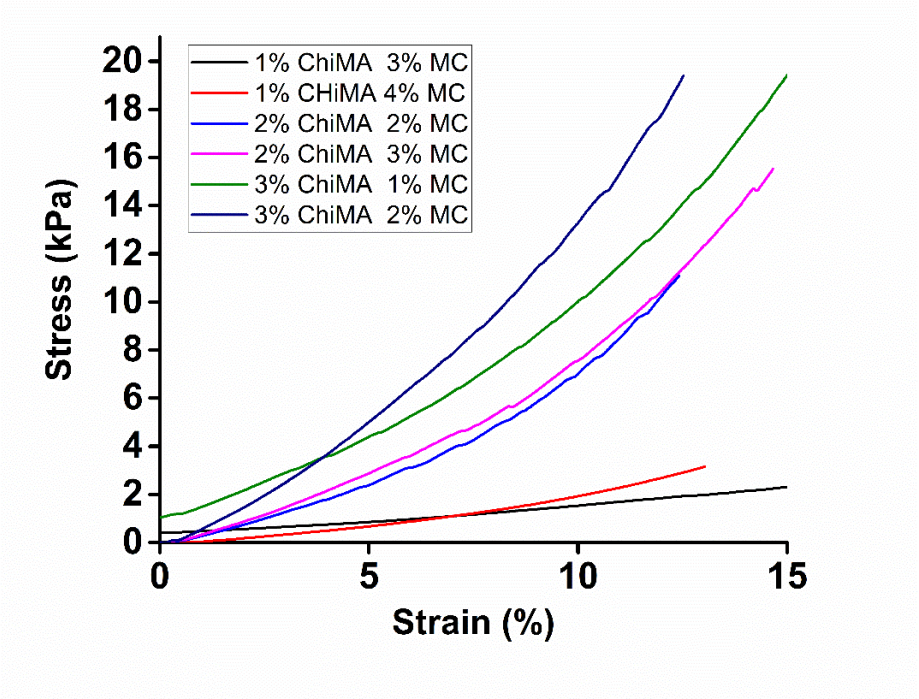


**Figure 3.7 Stress- Strain curves for the cast disks formed with six formulated inks.**

The compressive Young's moduli of ChiMA/MC hydrogels increased with increasing ChiMA concentration as a result of increased crosslinking density. The ChiMA content governs the degree of crosslinking and with increased number of crosslinking groups, a higher crosslinking density is thus achieved in the final scaffold. The Young's modulus of the ChiMA/MC hydrogels varies from 7 KPa to 65 KPa. A scaffold in tissue engineering needs to fill up a space otherwise occupied by natural tissue and provide a similar framework to regenerate the tissue (Drury and Mooney 2003). So, It is desirable to possess similar properties; especially mechanical properties as it would directly affect the function of the cells (Janmey and Miller

2011). Based on Figure 3.8 it possible to tune the ChiMA/MC to match the mechanical properties of skin in different locations in the range 5 KPa up to 65 KPa.

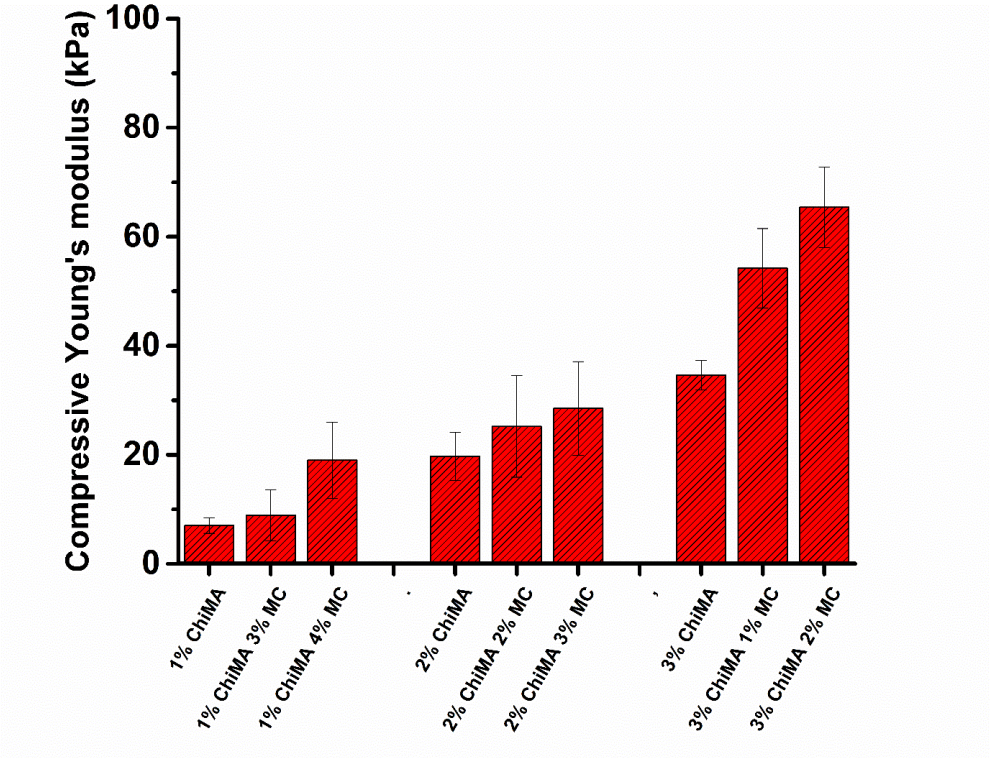


**Figure 3.8 Compressive Young's modulus for cast disks of formulated inks (mean ± SD, n ≤ 3).**

Moreover, all the crosslinked hydrogels were characterized by obtaining compressive Young's modulus in comparison with pure ChiMA hydrogels to verify the combined effect of ChiMA and methyl cellulose. From the results shown in Figure 3.8, there can be several conclusions. First, the mechanical strength of hydrogel increases with increasing ChiMA concentration. Secondly, there is a clear indication that adding methyl cellulose in the ink formulation improves the stiffness of the final hydrogel. Compared to the hydrogels prepared from ChiMA alone, the respective composite hydrogels prepared from ChiMA/MC exhibit higher compressive Young's moduli that appear to increase with increasing MC content. This could be due to the higher solid loading and enhanced hydrogen bonding between ChiMA chains and methyl cellulose chains.

### 3.3.2. Water uptake

The ability to absorb large amount of water and maintain a moist environment is one of the main properties that has to considered when employing hydrogels in wound healing applications (Aderibigbe and Buyana 2018). The absorbed water is also responsible for permeation of the nutrients into and cellular products out of the gel (Chirani, Gritsch et al. 2015). The water uptake capacity of a hydrogel depends mainly on the crosslinking network density (Yang 2012).

The ChiMA/MC hydrogel disks were freeze-dried and examined for their rehydration behaviour (Figure 3.9). All samples showed rapid rehydration behaviour, reaching equilibrium in less than 2 hours, with an equilibrium water uptake of more than 10-fold of their dry weight at room temperature. This indicates that all the ChiMA/MC hydrogels contain more than 90% water at equilibrium. The highest water absorption was shown by the hydrogels with 1% ChiMA3%MC and 1%ChiMA4%MC. This can be correlated with its low mechanical property as this directly corresponds to the compression test, where 1%ChiMA3%Mc and 1%ChiMA4%MC demonstrated weaker mechanical properties due to low ChiMA concentration. This finding is in agreement with the literature, which in simple terms states that fluid retention is inversely proportional to high mechanical properties (Dinoro 2016). With an increase in ChiMA concentration there can be an increase in steric hindrance due to higher crosslinking density and also an increase in hydrophobicity as a result of accommodating more hydrophobic methacrylate groups; both of which could lead to a decrease in the degree of swelling.

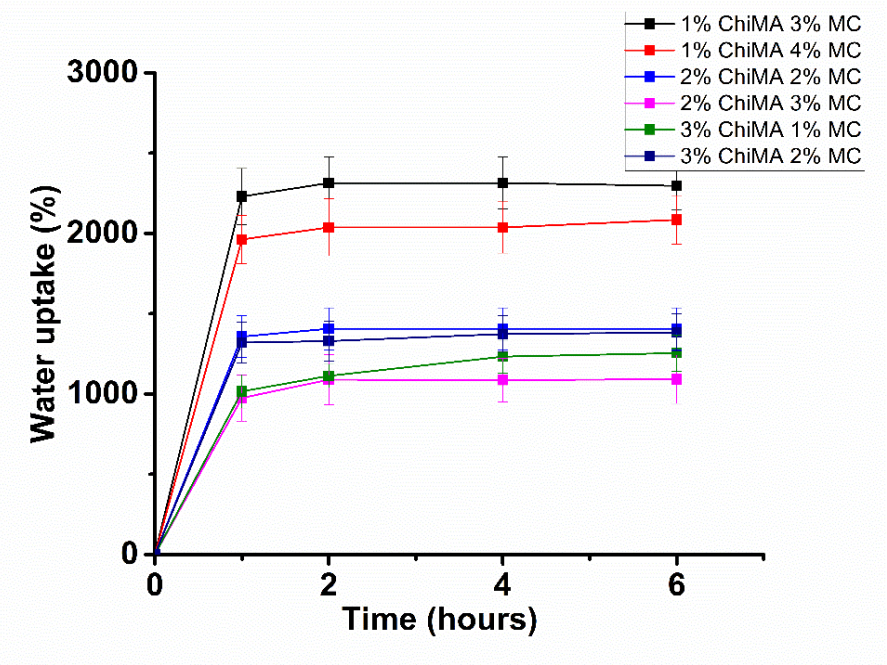


**Figure 3.9 Water uptake capacity for freeze- dried hydrogel cast disks made from six formulated inks (mean ± SD, n ≤ 3).**

### 3.3.3.Free polymer loss.

In order to determine which un-crosslinked polymer chains diffuses out of the scaffold, a free polymer loss experiment was done. The weight losses of the ChiMA/MC hydrogel cast disks were evaluated over time and compared with the pure ChiMA samples. The Results shown in Figure 3.10 indicate that there is no significant weight loss in pure ChiMA hydrogels. This suggests that the majority of ChiMA molecules are successfully crosslinked. By contrast, the samples prepared from ChiMA/MC show significant weight loss. With the information obtained based on pure ChiMA hydrogels, it can be concluded that the free polymer loss obtained for the ChiMA/MC samples is primarily a result of the release of entrapped methyl cellulose. This view is further supported by the weight loss result of ChiMA/MC hydrogels in subsequent study showing that the weight loss of ChiMA/MC hydrogels increases with increasing MC content with the exception of 1% ChiMA/4%MC. The latter exception may be due to experimental error caused by sample retrieval as the 1% ChiMA hydrogels were very weak and fragile. Another observation is that with the increase in ChiMA concentration in the

cast disk, a decrease in weight loss was also observed. This could be attributed to the higher crosslinking density associated with higher ChiMA concentrations, which sequesters more methyl cellulose chains.

Moreover, it could also be assumed that the release of methyl cellulose would create voids inside the scaffold which would facilitate the penetration of foreign materials such as enzymes and water (Gao, Gillispie et al. 2018). This will be further supported by the later experiment observation under in-vitro degradational studies in section 3.6. Hence, all the scaffolds made with ChiMA/MC may have voids within the structure that would facilitate gaseous exchange and water absorption and are especially useful properties for a wound dressing.

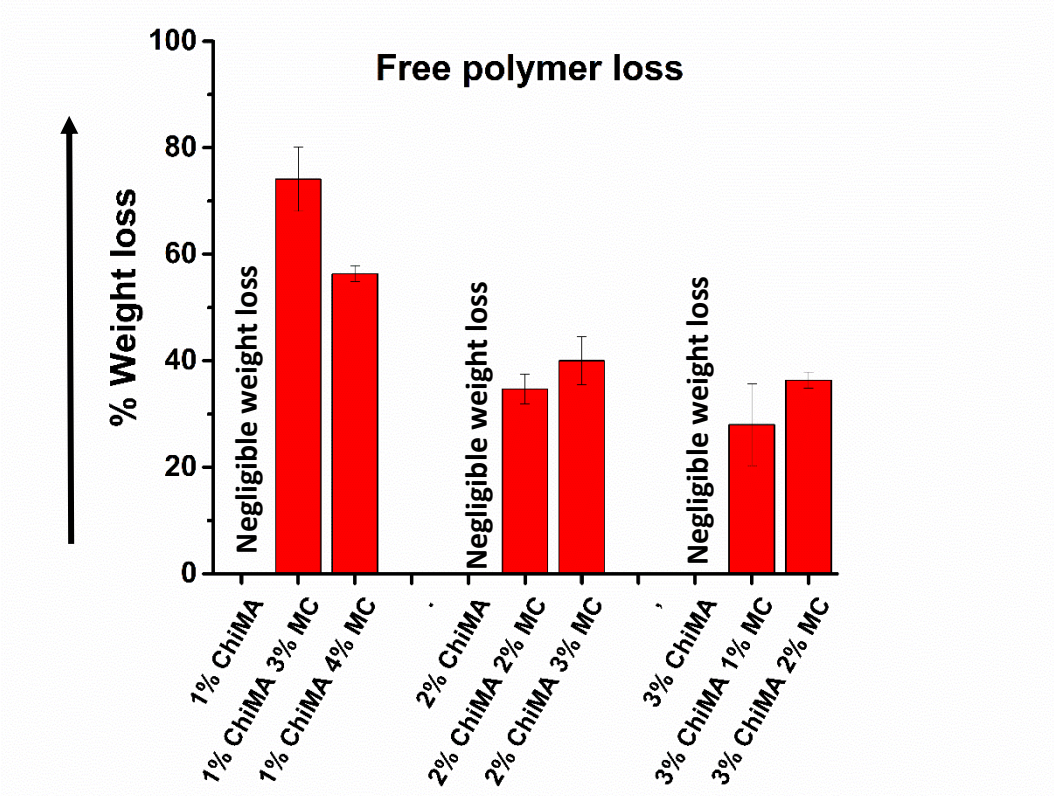


**Figure 3.10 Free polymer loss for cast disks of formulated inks as a percentage of weight loss (mean ± SD, n ≤ 3).**

All six ink formulations seem to have physicochemical properties that are useful for wound healing application, therefor final screening test was done to further narrow down.

## 3.4. Final screening test: Semi quantification assessment of printability by two-layer printing using bioplotter

The 6 ink formulations selected were subjected to final screening test using a semi-quantitative method reported by Ouyang, Yao et al. (2016). Semi-quantification assessment was carried out to explore the preliminary layer stacking ability of the printed structure. As explained in Section 3.2 it is one of the fundamental requirements for extrusion-based printing apart from extrudability which we confirmed through initial screening test. This will provide information on the layer stacking ability of the formulated inks through self-recovery characteristics upon deposition in order to maintain the desired structure. As in Figure 3.11 (A) for ideal printability, the interconnected channels of the printed construct would demonstrate a square shape where the Pr value would be 1 according to Equation 3 (Kyle, Jessop et al. 2017). If the Pr value is larger than 1 it is deemed as "over gelation" and less than 1 means "under gelation" where the filaments would fuse together, thus creating a circular shape instead of square shape. The closer that Pr values are to 1 demonstrates the bioink's ability to construct a design with more accuracy and precision to the designed model. Figure 3.11 (B) shows the maximum Pr value of each six of the ink's two-layer printings. It was found that only 2% ChiMA/3% MC and 3% ChiMA/2% MC biomaterial inks show the ideal gelation behaviour at room temperature. Although the other formulations were good at filament formation, they exhibited poor layer stacking, making them less effective at maintaining the printed structure.

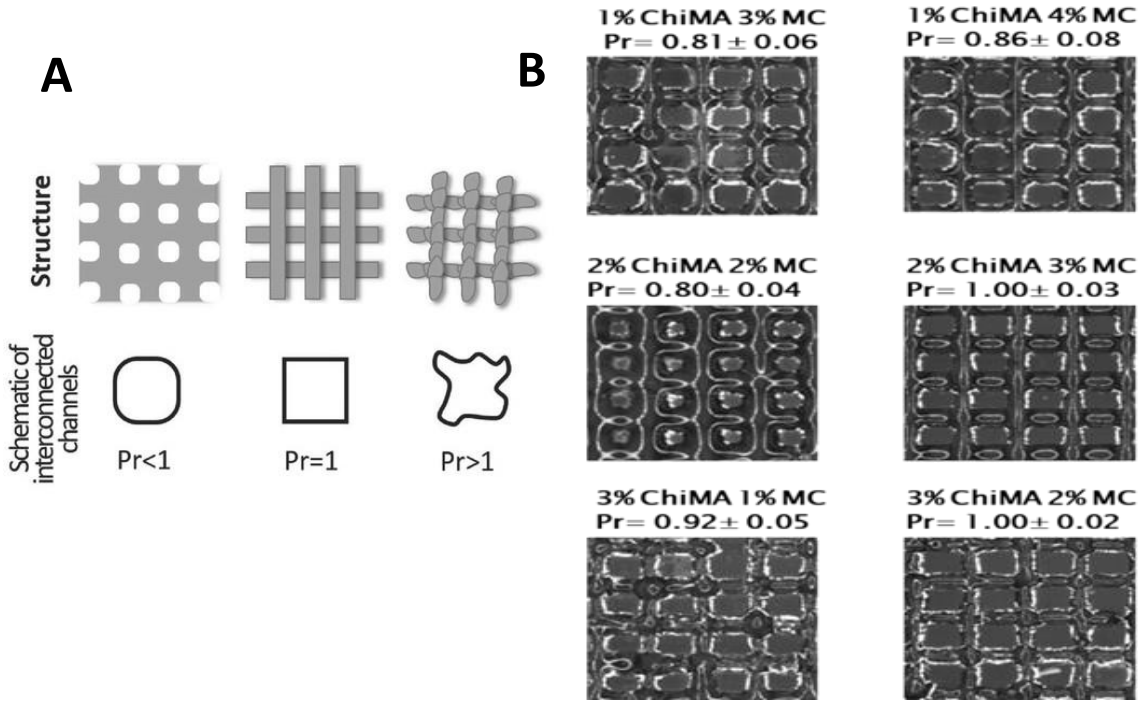


**Figure 3.11 (A) Evaluation of the printability of a biomaterial ink (Adapted from (Kyle, Jessop et al. 2017) (B) Experimental semi- quantification of printability for two-layer printing trials for selected six ink formulations at room temperature.**

Based on these findings, 2% ChiMA/3%MC and 3% ChiMA/2%MC ink formulations were selected for further analysis. Crosslinking kinetics and degradational studies were undertaken for the two selected ChiMA/MC inks before moving on to rheological studies.

## 3.5. Crosslinking kinetics by *in-situ* rheology.

In the presented work, post-printing UV crosslinking is essential in order to stabilize the 3D printed structures. Hence the information about the crosslinking kinetics of selected inks is vital to justify the efficiency of the crosslinking when building up a scaffold. Data was obtained to assess the 60 s UV exposure time for completion of the crosslinking process that was used to prepare cast disks with the photo-energy of 780 mJ. Only 2%ChiMA/3%MC and 3%ChiMA/2%MC formulations were assessed as they were selected from the screening test.

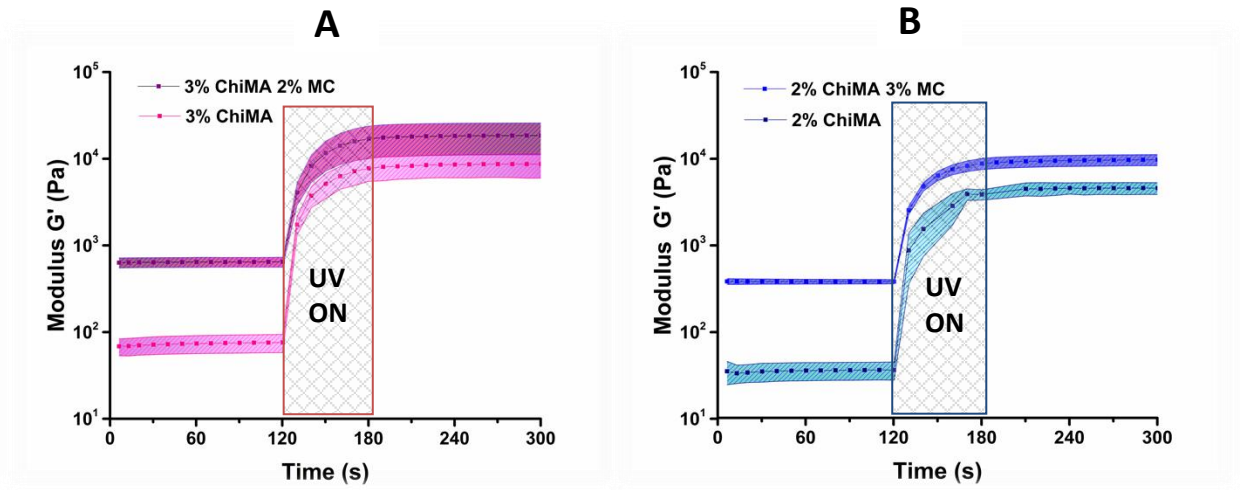


**Figure 3.12 In-situ rheology demonstrating the crosslinking kinetics of ChiMA/MC biomaterial inks and pure ChiMA: (A) Comparison of 3% ChiMA/ 2% MC biomaterial ink with 3%ChiMA solution; (B) Comparison of 2% ChiMA/3% MC biomaterial ink with 2% ChiMA solution.**

Figure 3.12 shows the *in-situ* photo-rheology data for the two identified lead ink formulations and corresponding ChiMA alone inks were also included for comparison. The evolution of the hydrogel network formation can be assessed by observing the crosslinking kinetics via *in-situ* rheology. Prior to UV crosslinking, the storage moduli of both composite inks were higher than the respective ChiMA alone ink. The storage moduli of both composition inks and ChiMA inks increased instantly upon exposure to the UV light (400 nm light source) initiating the photo-crosslinking process. It was observed that during the 60 s of UV exposure, the storage moduli reached to a plateau, which was also confirmed through observing the G' for a further 120s. This suggested a completion of photo-crosslinking at the end of 60 s irradiation time with total 780 mJ photo-energy and a 0.12% LAP photo-initiator concentration. Hence, the developed ChiMA/MC inks show rapid crosslinking profiles for extrusion-based printing.

In addition, the kinetics measurements were used to demonstrate the combined effects of ChiMA and methyl cellulose by comparing the ChiMA/MC crosslinking profile with pure ChiMA solutions. Both initial and Final storage moduli of the hydrogels, crosslinked from the

ChiMA/MC inks (2%ChiMA3%MC and 3%ChiMA2%MC), were higher than the corresponding hydrogels prepared from ChiMA only (2%CHiMA and 3%ChiMA), indicating the impact of MC on increasing the overall mechanical strength of the composite hydrogel. The higher storage moduli of ChiMA/MC hydrogels compared with respective pure ChiMA hydrogels suggested an added contribution of MC on the mechanical properties. This is likely a result of interactions between ChiMA and MC polymer chains including hydrogen bonding and hydrophobic interactions etc that reinforce the photo-crosslinked polymer network. This finding is also consistent with Sections 3.3.1 and 3.7.2 where inclusion of MC was shown to improve the overall mechanical stability of composite hydrogels.

## 3.6.In-Vitro degradation studies.

The degradation behaviour of a scaffold is important when developing a biomaterial ink as it directly affects the cell growth, tissue regeneration and host response (Ren, Yi et al. 2005). Chitosan has been shown to enzymatically degrade via lysosome, which is commonly present in human body fluids in various concentrations (Hankiewicz and Swierczek 1974, Hu, Hou et al. 2012). Lysozyme hydrolyses chitosan to produce chitooligomers. These chitooligomers are capable of activating the microphages and promoting collagen deposition to decrease the scarring in would healing applications. (Muzzarelli 1997, Kumar, Muzzarelli et al. 2004).

Degradation profiles of the ChiMA/MC hydrogels were evaluated in a lysozyme containing PBS solution at 37 $^{0}$C. Cast hydrogels disks prepared from two lead inks that were subjected to pre-treatment to eliminate the effect of weight loss due to the loss of free polymer. According to Figure 3.13, it was found that all the cast disks showed a faster degradation rate at an early stage and that over time the degradation rate slowed down, evidently by reaching a plateau or much slower degradation rate. Lysosome enzyme can only degrade ChiMA by hydrolysing the β 1-4 glycosidic bonds in the polymer chain and it cannot act on N-

acetylglucosamine, glucosamine units or crosslinking bonds (Han, Nwe et al. 2012, Guarino, Caputo et al. 2015). The initial high degradation rate can be due to the availability of β 1-4 glycosidic bonds, and as the degradation proceeds the number of β 1-4 glycosidic bonds decreases which in turn causes the degradation to slow down. Once all the β 1-4 glycosidic bonds are hydrolysed by the lysosome, the structures of scaffolds are still maintained by the chemical crosslinking that are responsible for the plateau and/or much slower degradation rates. Thus, ChiMA/MC scaffolds may not be able to be fully degraded by lysosome enzyme. It was also observed that both 3% ChiMA/2%MC and 2% ChiMA/3% MC hydrogels experience overall higher degradation as well as higher degradation rate compared to the pure 3% ChiMA and 2% ChiMA cast disks. This could be as a result of the release of uncross linked MC which is trapped inside the hydrogel cast disks along with the enzymatic degradation. In addition, the diffusion of free polymer out of the hydrogel may create spaces inside the 3%ChiMA2%MC and 2%ChiMA/3%MC scaffolds, as described in the previous Section 3.3.3, which makes those scaffold more susceptible to the enzymatic degradation than cast disks prepared from ChiMA alone.

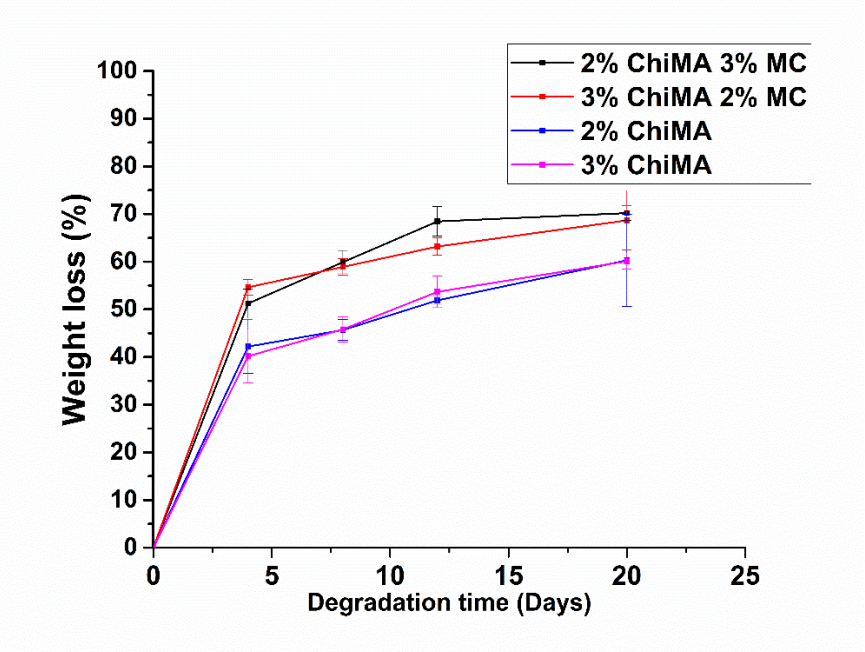


**Figure 3.13 Comparison of in-vitro degradation for hydrogel cast disks prepared from 2%ChiMA/3%MC, 3%ChiMA/2%MC, or ChiMA alone.( mean ± SD, n ≤ 3.)**

## 3.7.Rheological evaluation of the selected formulated inks

After the evaluation from the screening tests, two lead ink formulations (2%ChiMA/3%MC and 3%ChiMA/2%MC) were selected and the basic UV crosslinking profile and degradation profile were assessed. The next step is to carry out the rheological characterization. Especially in extrusion bioprinting, rheological demands placed on a biomaterial ink are very stringent as it has to be sufficiently viscous to enable production of continuous filaments, undergo shear thinning, low yield stress to enable ease of flow under pressure, and the rapid self-recover upon deposition. In other words, extrusion based 3D printing correlates with rheology in all the main stages of biomaterial printing (Liu, Bhandari et al. 2019). Herein, this is discussed further below around the influence of a number of important rheological aspects of the ChiMA/MC biomaterial ink such as shear thinning, yield stress, self-recovery ability and the effect of temperature on the viscosity of the material.

### 3.7.1.Shear thinning behaviour and yield stress measurements

Shear thinning is the decrease in viscosity with the increase in shear stress in non-Newtonian fluids, as it is often the case with the majority of high molecular weight polymer solutions due to the reorganization of the entangled polymer chains along the shear direction (Malda, Visser et al. 2013). This shear thinning behaviour is useful in nozzle-based applications, as it decreases the tendency of nozzle clogging thereby promoting continuous filament formation, and decreases the stress exerted upon the biomaterial ink that can improve cell survival in the case of cell printing (Hölzl, Lin et al. 2016).

The shear- viscosity properties of the two selected ChiMA/MC inks are shown in Figure 3.14. Both inks showed shear thinning behaviour, which can be fitted to a power law as given in Equation 5. This equation can be used to calculate the shear thinning coefficients to predict the optimal printing conditions, as shown below in Section 3.8.

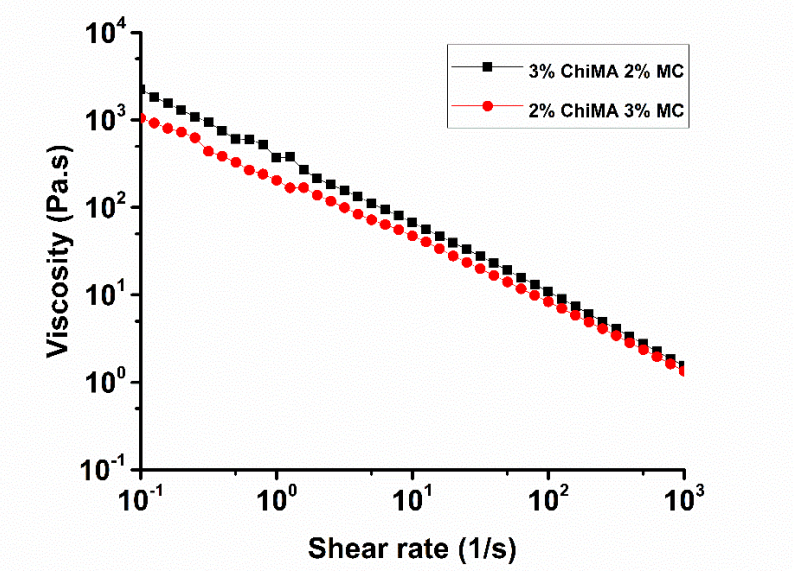


**Figure 3.14 Shear-viscosity property of two identified formulated biomaterial inks**

The yield stress gives insight into the minimum stress that should be applied for the material to flow or, in other words, the minimum stress above which the material will exhibit more of liquid-like properties rather than solid properties( G”>G’) (Menger and Peresypkin 2003, Siqueira, Kokkinis et al. 2017). This yield stress should be below the maximum shear stress generated by the nozzle (plug flow regime) for the materials to be used in printing. The maximum shear stress is generated at the wall of the nozzle and it can be calculated by using Equation 14; where **Δ**P is the maximum pressure that can be applied by the printer, r is the radius of the nozzle and L is the length of the nozzle. (Siqueira, Kokkinis et al. 2017)

**Equation 14| determination of the radial shear stress within the deposition nozzle (τ)**

$$\tau = \frac{\Delta P}{2L} r$$

By applying the pressure values in accordance with the EnvisionTEC bioplotter and the radius of the smallest nozzle that was considered in this study (**Δ**P= 5 × $10^5$ Pa; r = 1×$10^{-4}$ m; and L = 0.0134 m), the maximum shear stress was found to be 1865.7 Pa. The storage modulus (G’) and loss modulus (G”) profile measured with a logarithmical shear stress ramp to determine the yield stress is shown in Figure 3.15. The yield stress of 3% ChiMA/2% MC ink and 2%

ChiMA/3% MC was found to be 325.6 Pa and 163.1 Pa, respectively. The yield stress values were well below the plug flow which is consistent with the screening test results in support of the printability of the two inks.

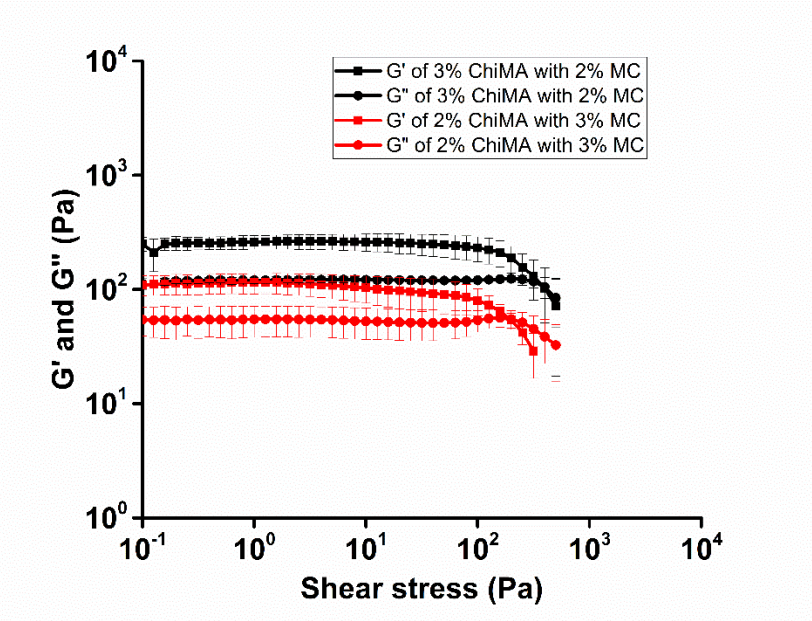


**Figure 3.15 Oscillatory rheological measurements for the two biomaterial inks at 25ºC, 1 Hz frequency and 0.1 % strain (mean ± SD, n ≤ 3).**

### 3.7.2. Temperature sweep

Methyl cellulose is a thermo-responsive material which shows a distinct sol-gel phase transition when heated (Chen, Chang et al. 2007). To determine if the selected inks retain the similar thermo-responsive characteristics as with MC, a temperature sweep was carried out for the biomaterial inks along with ChiMA and MC.

As shown in Figure 3.16 (A), at low temperature the 3% methyl cellulose shows a G" higher than G' and with the increase in temperature G' becomes higher than G". When the storage modulus (G') is greater than the loss modulus (G"), the material exists as an elastic gel/solid, and when G" dominates the material is described as a viscous liquid (Menger and Peresypkin 2003). So, at low temperatures MC behaved as a viscous liquid and with the increase in temperature it underwent a sol-gel transition at around 25 $^{o}$C which now has more like gel characteristics. Both the 2%ChiMA/3%MC ink and the pure 2%ChiMA have more gel-like

character, as G' is higher than that of G" throughout the temperature range. However, the storage modulus of the 2%ChiMA3%MC inks tends to increase after 25 $^{o}$C because of the effect of MC in it.

The trend for 3%ChiMA2%MC ink, 3%ChiMA and 2%MC is shown in Figure 3.16 (B) are same as above except, unlike 2%ChiMA3%MC, 3%ChiMA2%MC shows less dependent on the temperature. This could be due to low MC content in the overall weight. It can also point out that the 3%ChiMA2%MC ink has lower storage modulus compared to 2%ChiMA3%MC ink which can be an indication of a less entanglements thus a higher mobility in 3%ChiMA2%MC ink. This will be further proven in a latter self-recovery Section 3.7.3.

More importantly, in both Figures 3.16 A and B, the composite biomaterial inks (3%ChiMA/2%MC and 2%ChiMA/3%MC) show higher G' and G" than those of individual constituent alone (ChiMA or MC) at the same respective concentration. Again, this indicates the reinforcement of rheological properties due to interactions between the two constituent materials.

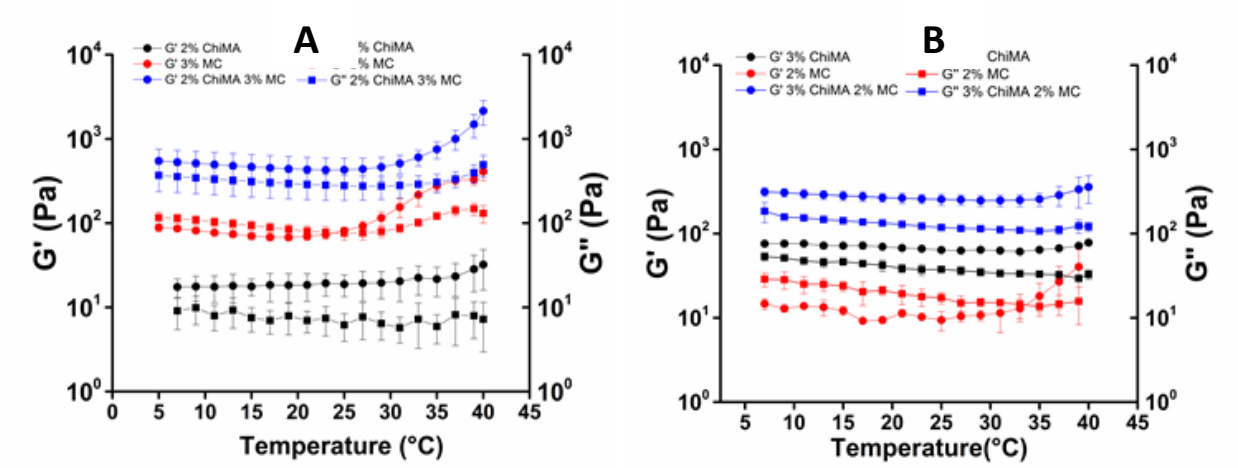


**Figure 3.16 Rheological temperature scans from 5°C to 40°C with a 2°C/min constant heating rate (mean ± SD, n ≤ 3). A) Temperature sweep for 2%ChiMA/3%MC, 2%ChiMA and 3%MC. B) Temperature sweep for 3%ChiMA/2% MC, 3%ChiMA and 2%MC.**

### 3.7.3. Self-recovery ability

Extrudability of a biomaterial ink can be determined by parameters such as viscosity, shear thinning and the yield stress. However, shape fidelity of the printed filament depends on how fast the material can reinstate the network after removal of the shear stress. This self-recovery ability was examined by performing a recovery test. To mimic the printing process, a low shear rate of 0.01 $s^{-1}$ was selected to represent the rest condition, followed by a sudden increase of shear rate to 1000 $s^{-1}$ to simulate the process of ink passing through the nozzle. This process was repeated 3 times, during which the viscosities of the two inks were recorded as a function of time.

As shown in Figure 3.17, both inks showed a rapid recovery after the application of higher shear rate. When exposed to high shear stress, the viscosity decreased from 750 Pa to 0.7 Pa for the 2%ChiMA/3%MC ink, and from 960 Pa 50 1.2 Pa for the 3%ChiMA/2%MC ink. Upon returning to the low shear rate (0.01 s-1), the samples recovered their viscosity within seconds but with a decreased viscosity compared with its original value. 2%ChiMA/3%MC regained up to 52.8% of its previous value, and 3%ChiMA/2% MC regained 83% immediately and reached its original value of viscosity within 2 minutes. This could be a result of less entanglements in 3%CHiMA2%MC ink compared to 2%ChiMA3%MC. This observation is consistent with the temperature sweep in section 3.7.2. During the second cycle, 2%ChiMA/3%MC regained almost 100% of its previous value and 3%ChiMA/2%MC regained only 63% of its previous value. Finally, during the third repetition both the biomaterial inks recovered to their original values. The overall decreasing viscosity with time under shear stress phenomenon can be interpreted as the thixotropic behaviour of the material (Müller, Becher et al. 2015).

Depending on the overall results, it can be concluded that the ChiMA/MC biomaterial inks have favourable rheological properties to be used in extrusion based biofabrication applications

as they have rapid self-recovery characteristics which is crucial to retain the structure until post-curing.

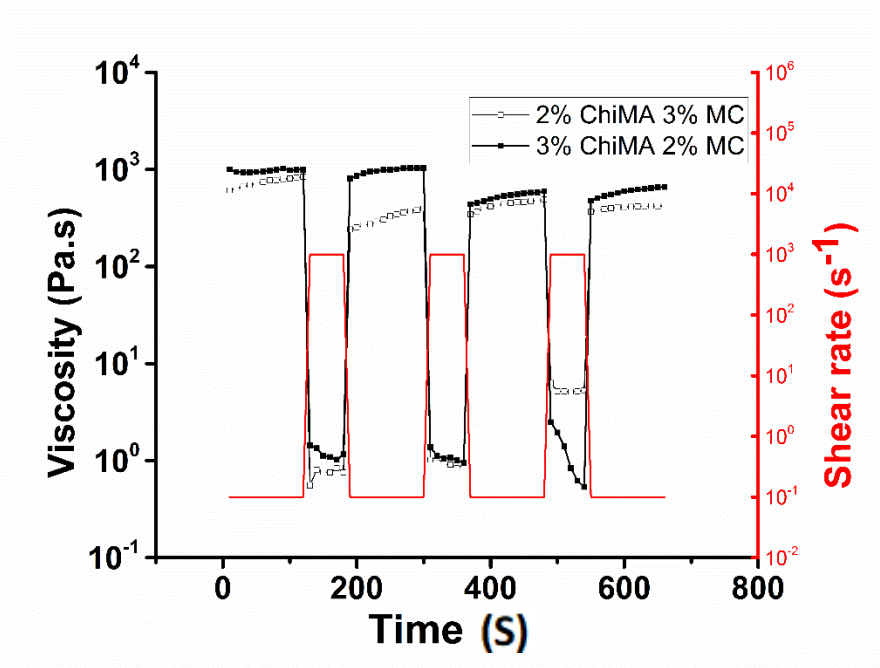


**Figure 3.17 Step strain measurement of 2%ChiMA/3%MC and 3%ChiMA/2%MC during sudden increase in shear rate from 0.1 $s^{-1}$ to 1000 $s^{-1}$ with time sweep.**

## 3.8. Window of Printability- A theoretical approach

In the context of bioprinting, optimization of a newly developed biomaterial ink or adapting an established biomaterial ink with existing operating parameters that are available could be challenging as well as time consuming (Paxton, Smolan et al. 2017). A mathematical model developed by Paxton, Smolan et al. (2017) was used to address this issue by modelling the extrusion printing process to calculate the average extrusion velocity based on operating parameters and shear thinning coefficients. The operating parameters here are pressure, needle length and diameter. The shear thinning coefficients were calculated by obtaining the shear viscosity profile of each ink at printing temperatures and plotted viscosity with respect to shear rate on logarithmic axes and applying a Power Law regression in the form of **Equation 5** to the initial linear region of the slope. The desired printing temperature was experimentally found

to be 18 $^0$C for 3% ChiMA/2% MC and 25 $^0$C for 2%ChiMA/3% MC. The calculated shear thinning coefficients at desired printing temperatures are as per table 3. Average extrusion velocity was calculated for an ink according to the developed equation 7, within a range of operating parameters (Ex: Pressure 1 Bar to 5 Bar, Needle diameter – 100, 125 and 165 µm). The 'Window of printability' was then defined by selecting the values within 1 to 20 mm $s^{-1}$ which was based on the experimental expertise of the bioplotter that was used to achieve a high shape fidelity within feasible time frame.

The theoretical model has its limitations, as it is formulated based on several assumptions such as friction free laminar flow, non-slip boundary conditions and independence from the temperature factor that alters the viscosity of a material. Therefore, it is recommended to use this as a starting point of characterization to identify possible ink formulations suitable for the operating parameters. This should then be followed up by experimental optimization by using the printer. However, to minimize the temperature factor, the shear thinning coefficients were found at the desired printing temperature.

The bioprinting window for the two formulated biomaterial inks are shown in Figures 3.18 (A) and 3.19 (A), where the blue colour represents an extrusion velocity that is too slow (>1 mm/s) and red colour represents the velocities above 20 mm/s that lead to very high printing speeds, resulting in less precision in printing. Additionally, the theorical extrusion behaviour of the biomaterial ink inside the nozzle was plotted to understand how the extrusion velocity and shear rate differs across the needle. Extrusion velocity and shear rate across the needle were calculated using the Equations 6 and 11, respectively.

**Table 3 Calculated values for the shear thinning coefficients**

| Formulated ink | Printing temperature | n | K |
|---|---|---|---|
| 3% ChiMA 2% MC | 18 °C | 0.24 ± 0.05 | 354 ± 45 |
| 2% ChiMA 3% MC | 25 °C | 0.32 ± 0.07 | 242 ± 64 |

Predictions using the window of printability suggests that both the ink formulations can be printed across a wide range of operating parameters of the bioplotter, even using different nozzle sizes. According to Paxton, Smolan et al., the window of printability mainly depends on the shear thinning coefficients that differ significantly depending on the material. So, the size of the window of printability is quite similar for the two formulated biomaterial inks.

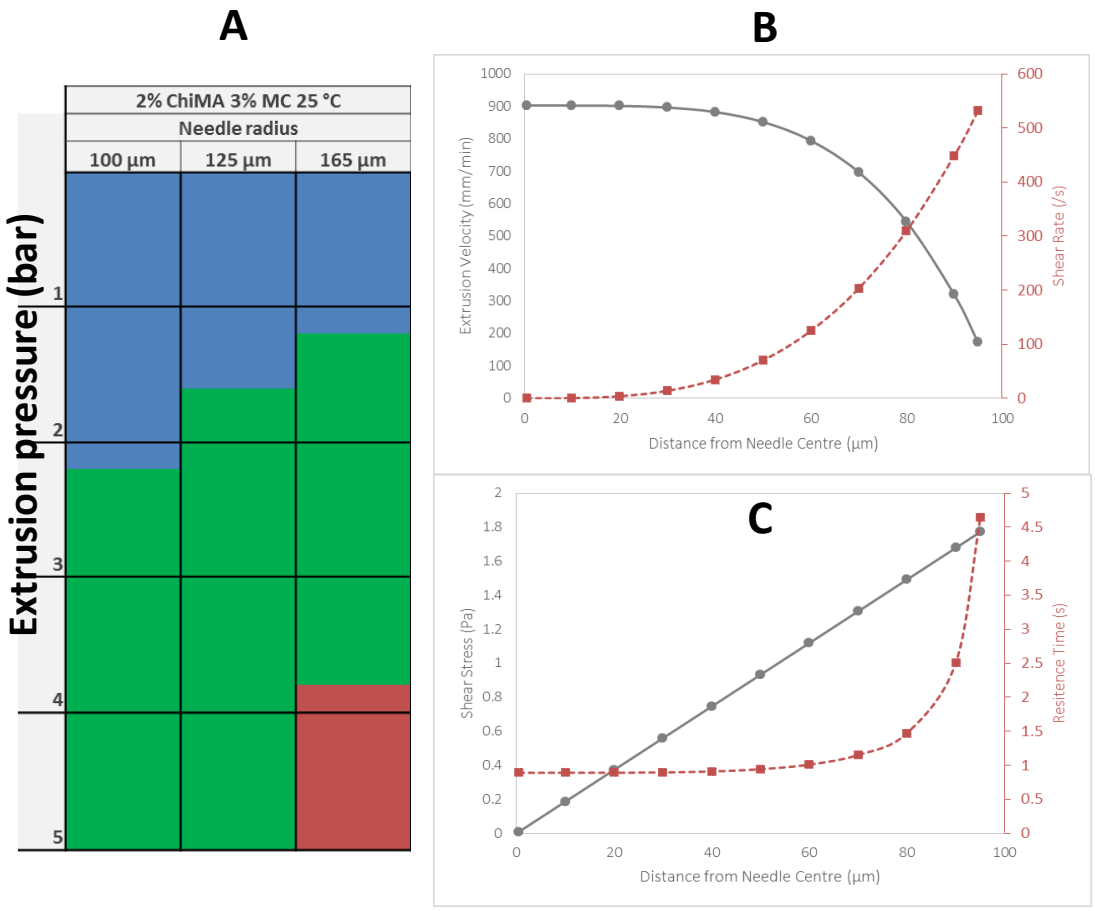


**Figure 3.18 A) Bioprinting window for 2% ChiMA/3%MC biomaterial ink at 25 ºC. (B) Theoretical extrusion velocity and shear rate across the inner radius of the printing needle at 5 Bar. (C) Theoretical residence time across the inner radius of the printing needle at 5 bar.**

Figure 3.18 (B) (C) and Figure 3.19 (B) (C) show the distribution of shear factor across the needle. The shear rate increases exponentially towards the needle wall. The shear stress distribution increases linearly from a minimum along the centre to the maximum by the needle wall. The highest stress with longest residence time is exerted in the immediate vicinity of the

wall. The overall evaluation would give an idea of the extrudability as well as the shear stress to determine the cytocompatibility of the printing process that would be important for future work towards cell printing.

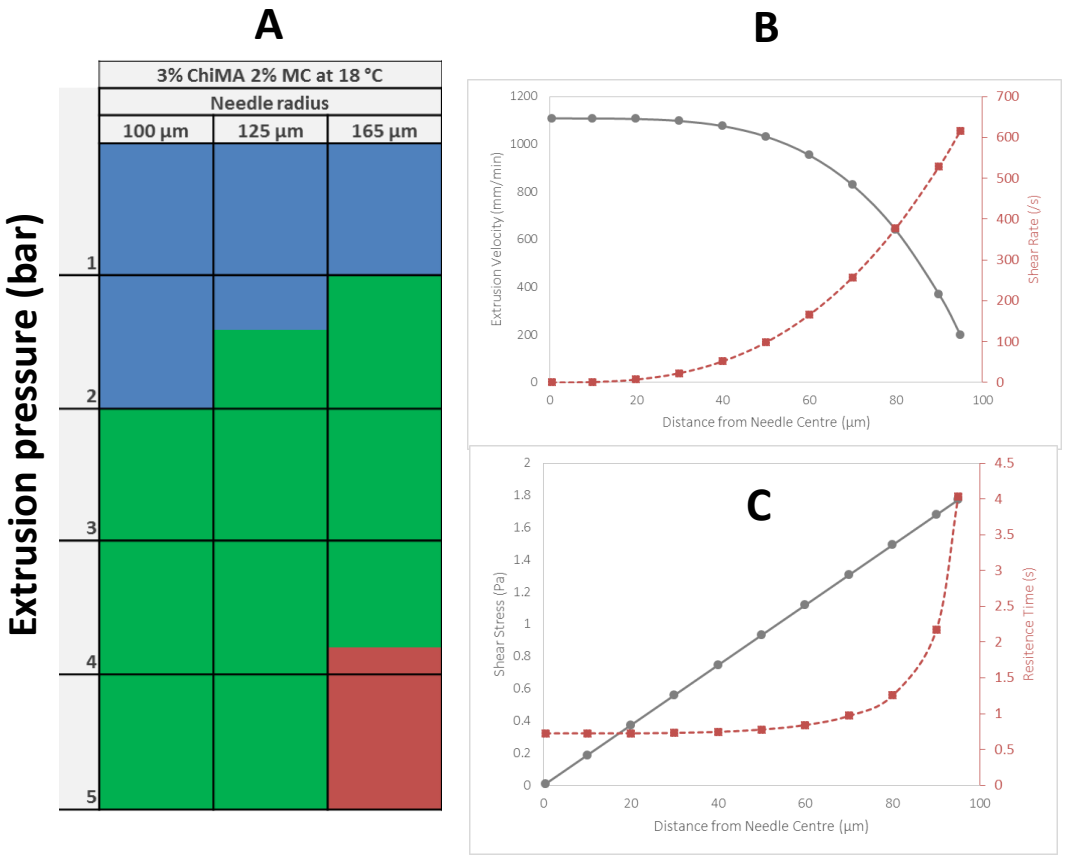


**Figure 3.19 (A) Bioprinting window for 3% ChiMA/2%MC biomaterial ink at 18 ºC. (B) Theoretical extrusion velocity and shear rate across the inner radius of the printing needle at 5 Bar. (C) Theoretical residence time across the inner radius of the printing needle at 5 bar.**

This model can be used as simple and rapid characterisation of an ink as well as to minimize the trial and error approach when optimisating an ink for any extrusion bioprinter within its operating parameters.

## 3.9.Printing evaluation.

Finally, the formulated ChiMA/MC biomaterial inks' printing capability was investigated by quantitative analysis of the printed filament diameter and by assessing correct reproduction of different CAD designs shapes.

### 3.9.1. Structure diameter evaluation with print speed.

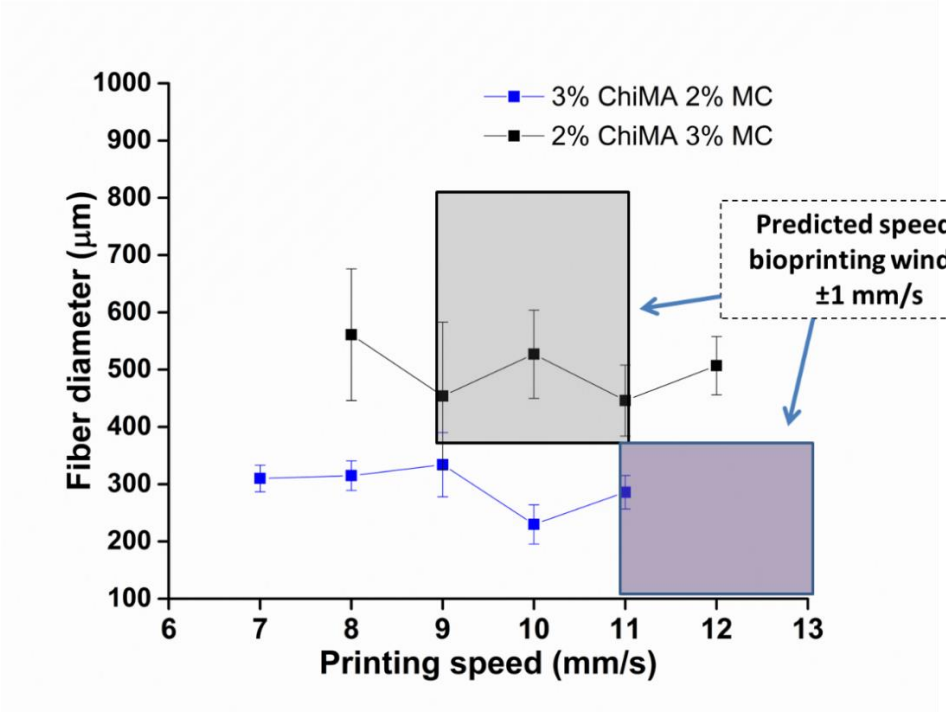


**Figure 3.20 Average strut diameter of 2 layer printing of formulated inks with A-27 gauge needle (internal diameter 200µm) at 5 bar pressure. 3% ChiMA/2%MC was printed at 18 $^0$C and 2%ChiMA/3%MC was printed at 25 $^0$C (mean ± SD, n ≤ 3).**

Evaluation of strut diameter is a quantitative measurement of gauging the printing resolution. Strut diameter of a printed filament can be dependent on many factors, including the material properties, extrusion temperature, needle diameter, extrusion speed and pressure. Although it was concluded that the inks' printability cannot be significantly increased by varying the temperature (Section 3.4.2), it was found experimentally that the 3%ChiMA/2%MC ink extrudes easily without clogging at a lower temperature. So 3%ChiMA/2%MC biomaterial ink was printed at 18 $^0$C while 2%ChiMA/3%MC biomaterial ink was printed at room temperature for assessing the strut diameter. Furthermore, for the purpose of comparison, both the

formulated inks were printed at the same pressure (5 bar) using the same needle diameter (200 µm) with varying printing speeds; and the strut diameter was calculated via ImageJ software. Figure 3. 20 showed that the 3%ChiMA/2%MC biomaterial ink has better resolution in printing compared to 2%ChiMA/3%MC, as the former has a strut diameter closest to the needle diameter. Although both the biomaterial inks have the same solid loading, 3%ChiMA/2%MC has higher concentration of crosslinkable material (ChiMA) thus displays rheological properties that enable better printing resolution. This finding is further demonstrated upon 8-layer printing of a scaffold, as outlined in Section 3.9.2 below.

To elucidate the validity of the predicted values in the theoretical bioprinting window section under practical printing conditions, the range of predicted speed value ± 1 mm/s is marked in the same Figure 3.20. For the 2%ChiMA/3%MC biomaterial ink, the theoretical predicted value correlated well with the practical value. But for the 3%ChiMA/2%MC biomaterial ink, the predicted value overestimated the extrusion velocity, hence there was poor correlation. This has been the case in the original study as well explained by Paxton, Smolan et al., that it could be due to the difficulty in matching the collector speed and extrusion velocity, as well as assumptions of the model (friction free laminar flow and non-slip boundary conditions). Nevertheless, the theoretical approach for determining the window of printability is shown to be beneficial in developing and optimizing the biomaterial inks. It significantly reduces the time consumed in developing a biomaterial ink by minimizing the trial and error approach. It is also important to note that this model acts as a mere guide to rapid selection of suitable printing conditions of a biomaterial ink and that it must be validated through the use of a bioprinter to determine the ideal printing parameters.

### 3.9.2. Printing complex geometries

The main structure used for printing the scaffold is shown in Figure 2.2. Two formulated

biomaterial inks were used to print up to 8 layers and the results are shown in Figures 3.21 and 3.22.

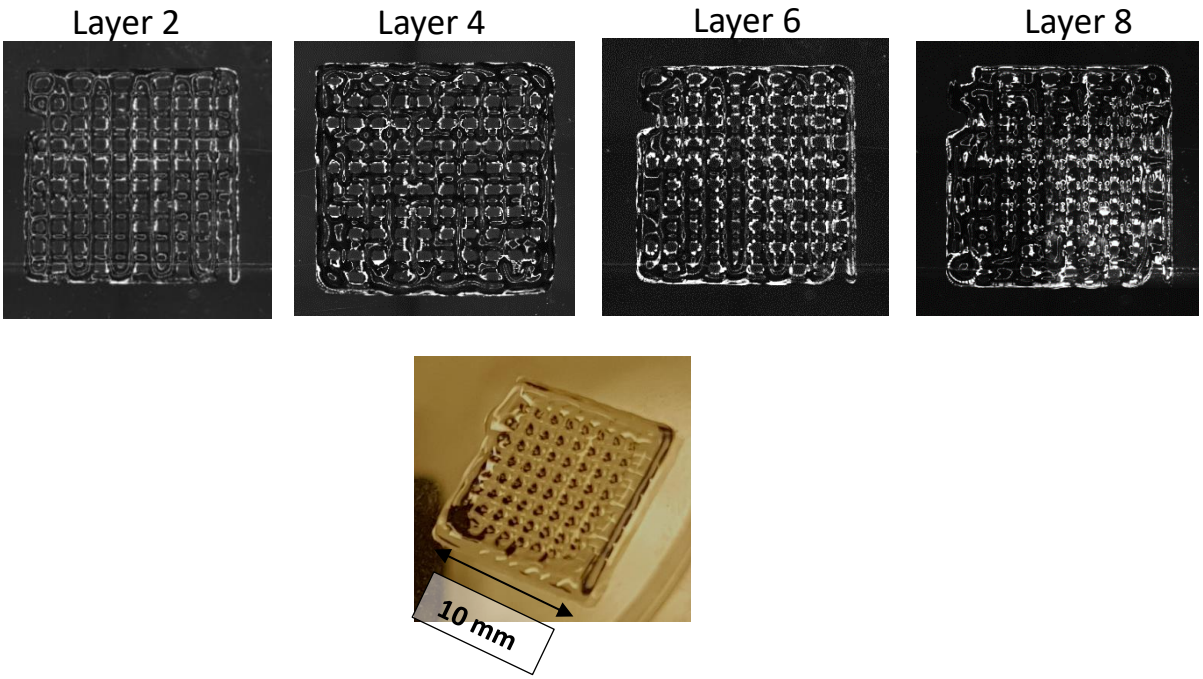


**Figure 3.21 2% CHiMA/3%MC printing scaffold up to 8 layers.**

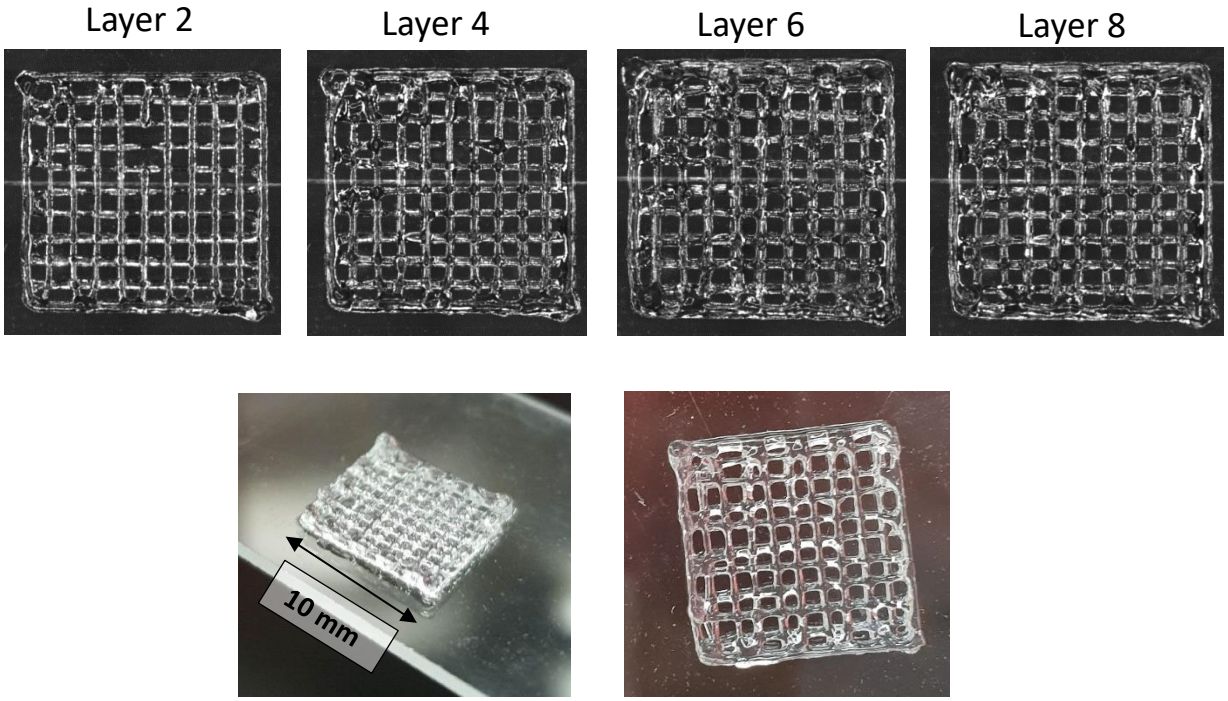


**Figure 3.22 3% ChiMA/2%MC printing scaffold up to 8 layers.**

Although the selected two biomaterial inks show the same printability (Pr value) from the screening tests, it was found experimentally that the 3% ChiMA/2%MC has a better shape fidelity over the 2%ChiMA/3%MC. This could be attributed to the fact that the 3% ChiMA/2%MC biomaterial ink has more crosslinking sites, leading to a higher crosslinking density to hold the structure together more effectively. Considering all the factors, it can be concluded that the 3%ChiMA/2%MC biomaterial ink has improved rheological and mechanical characteristics to be used in extrusion-based 3D printing. This is further supported by the reproduction of different shapes using 3%ChiMA/2%MC biomaterial ink, as shown in Figures 3.23 and 3.24. Both the shapes were able to be successfully printed with up to 8 layers.

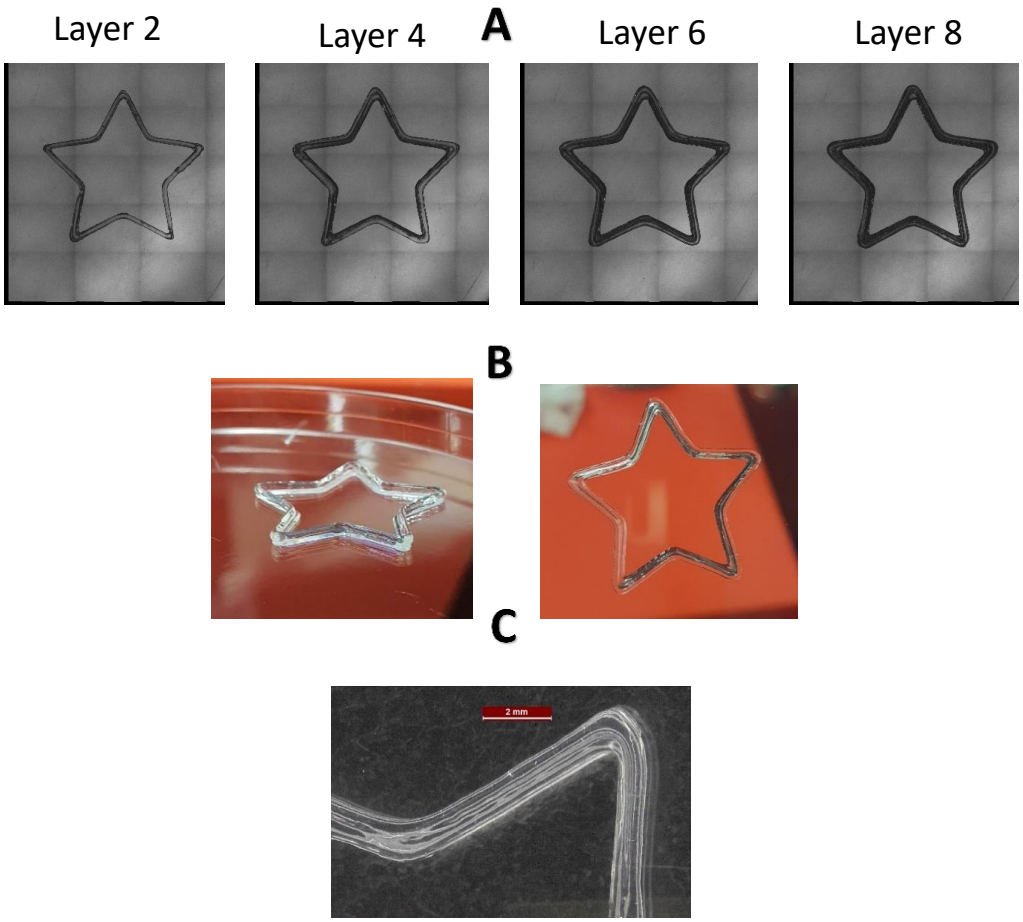


**Figure 3.23 (A) The layer progression of star shape structure with the EnvisionTEC 3D-Bioplotter captured with the inbuilt bioplotter camera. (B) Images on final print. (C) Optical microscopic image of highlighted printed area**

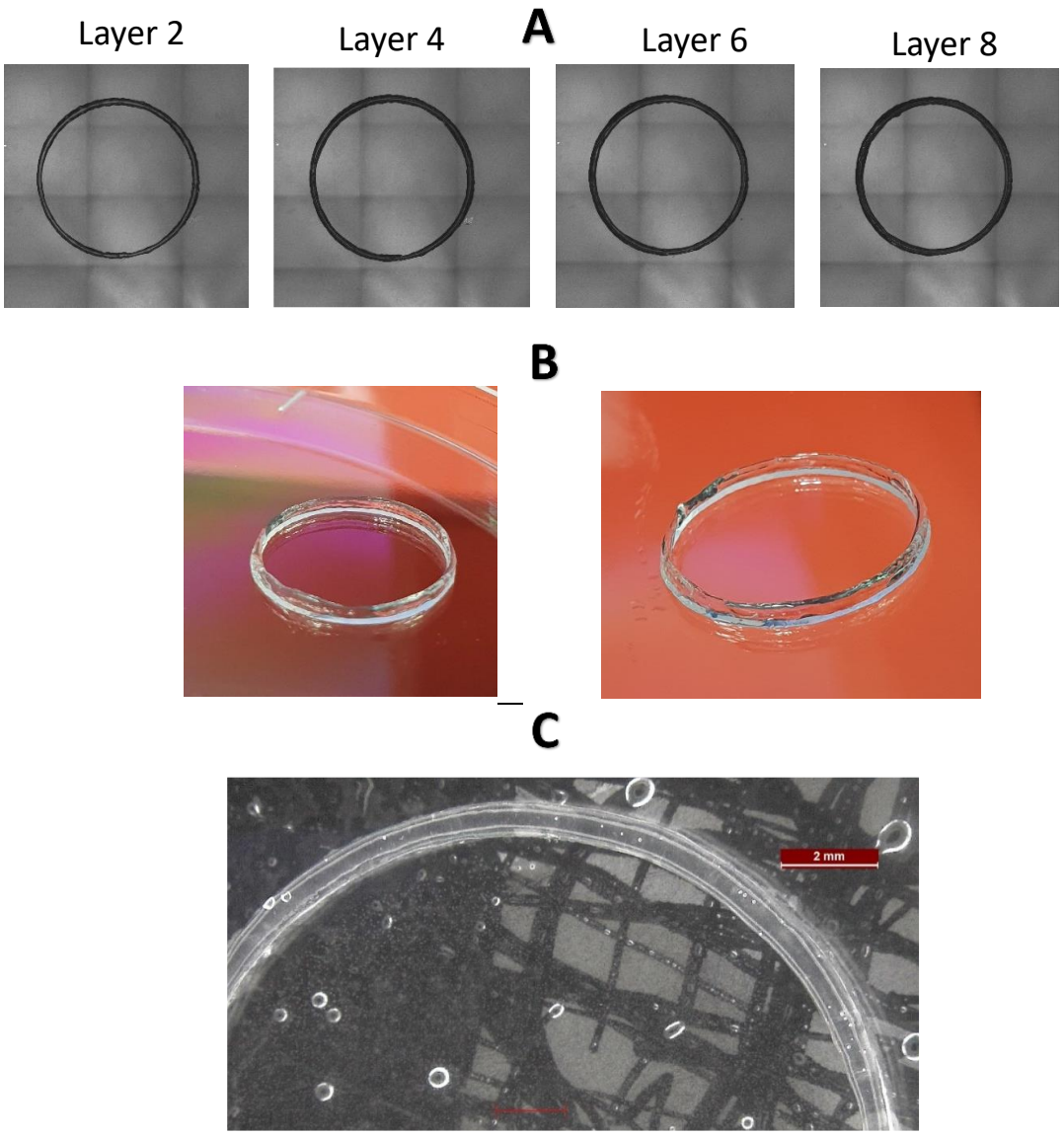


**Figure 3.24 (A) The layer progression of cylinder shape structure with the EnvisionTEC 3D-Bioplotter captured with the inbuilt bioplotter camera. (B) Images on final print. (C) Optical microscopic image of highlighted printed area.**

## 3.10.Preliminary cytocompatibility studies of 3D printed 3%ChiMA2%MC & 2%ChiMA3%MC hydrogels

The final step is to assess the cytocompatibility of the printed scaffolds. As the intended application is in wound healing, preliminary studies for cell attachment and survival were carried out using in-vitro cell culture of human dermal fibroblasts (HDFs) in 3D printed scaffolds. Human dermal fibroblasts were selected due to their prominent role in the proliferation and remodelling phases in wound healing (Lo, Hu et al. 2015). Figures 3.25 and 3.26 show the fluorescent images of HDFs cultured in 3D printed scaffolds using 2%ChiMA/3%MC and 3%ChiMA/2%MC, respectively. Live cells were stained green using calcein AM and the dead cells were stained in red using propidium iodide. The cells cultured in both scaffolds were shown to be viable, but with poor cell attachment. Compared to day 1, there is a reduced number of cells in both scaffolds at day 7. They tended to form aggregates with rounded morphology, which may be due to lack of cell binding sites in the matrix resulting in poor cell-matrix interactions (Gaharwar, Rivera et al. 2013). These cell-matrix interactions either could be electrostatic interaction and/or integrin bonding (Khalili and Ahmad 2015). This is consistent with the literature where Sayyar, Gambhir et al. shows that the fibroblasts seeded on ChiMA have similar results where cells did not adhere to the surface and aggregattion of the cells were observed. So, the overall results indicate that there is no cytotoxicity in the components of the CHiMA/MC hydrogels.

However, cell-hydrogel interactions can be improved by incorporating cell adhesion moieties like RGD peptides (Hersel, Dahmen et al. 2003) and collagen etc(Gansau and Buckley 2018).

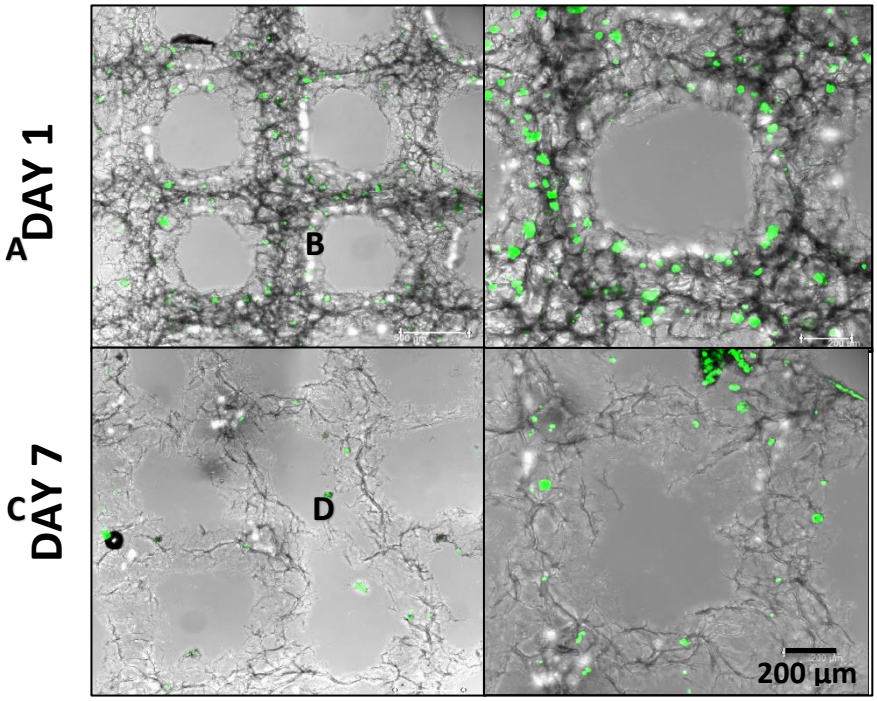


**Figure 3.25 Live and dead cells staining images of human dermal fibroblasts cultured on the 3D printed 2%ChiMA/3%MC hydrogel scaffold at day 1 (A, B) and day7 (C, D).**

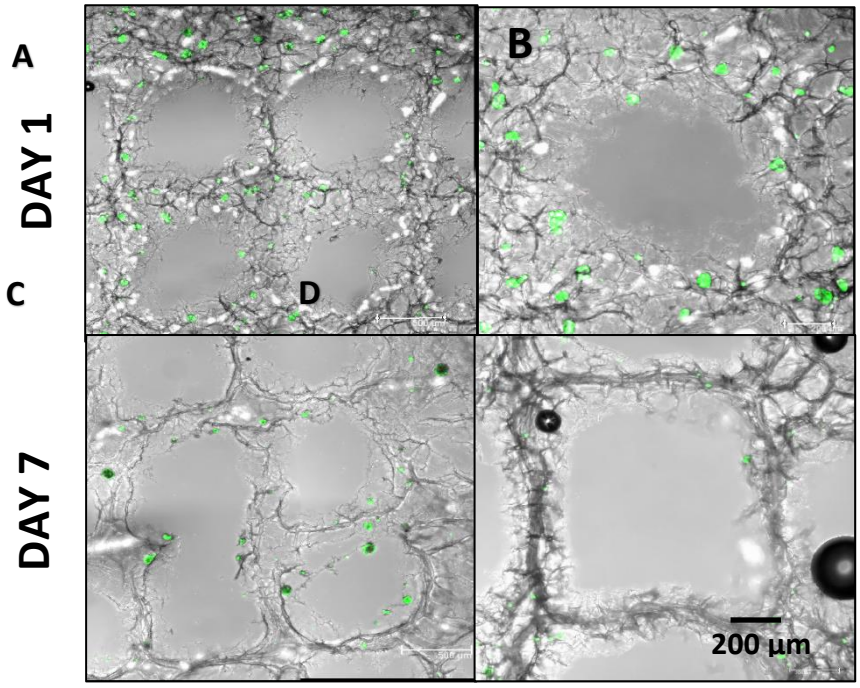


**Figure 3.26 Live and dead cells staining images of human dermal fibroblasts cultured on the 3D printed 3%ChiMA/2%MC hydrogel scaffold at day 1 (A, B) and day 7 (C, D).**

In this work, collagen type I was coated on ChiMA/MC printed scaffolds to enhance the cell-matrix interactions. Collagen was neutralized according to the manufacturer's instructions (SANTA CRUZ BIOTECHNOLOGY, INC sc-136157) and this process was maintained at 0-4 $^{o}$C. The ChiMA/MC printed scaffolds were freeze-dried and soaked in the collagen solution, and then further incubated at 37$^{0}$C for an hour. This allows gelation of collagen to take place to form insoluble collagen fibres within the 3D printed polymer matrices. Comparing the live cells in Figure 3.25 and 3.26 to Figure 3.27, the incorporation of collagen increases cell attachment as it shows more live cells at day 1. The cells are also shown to attached well with the modified matrix, with elongated shapes rather than round morphology. In contrast to the scaffold without Collagen (Figure 3.25 and 3.26), Collagen incorporated scaffold (Figure 3.27) showed increase numbers of cells at day 7 compared to day 1, suggesting the matrix support cell proliferation.

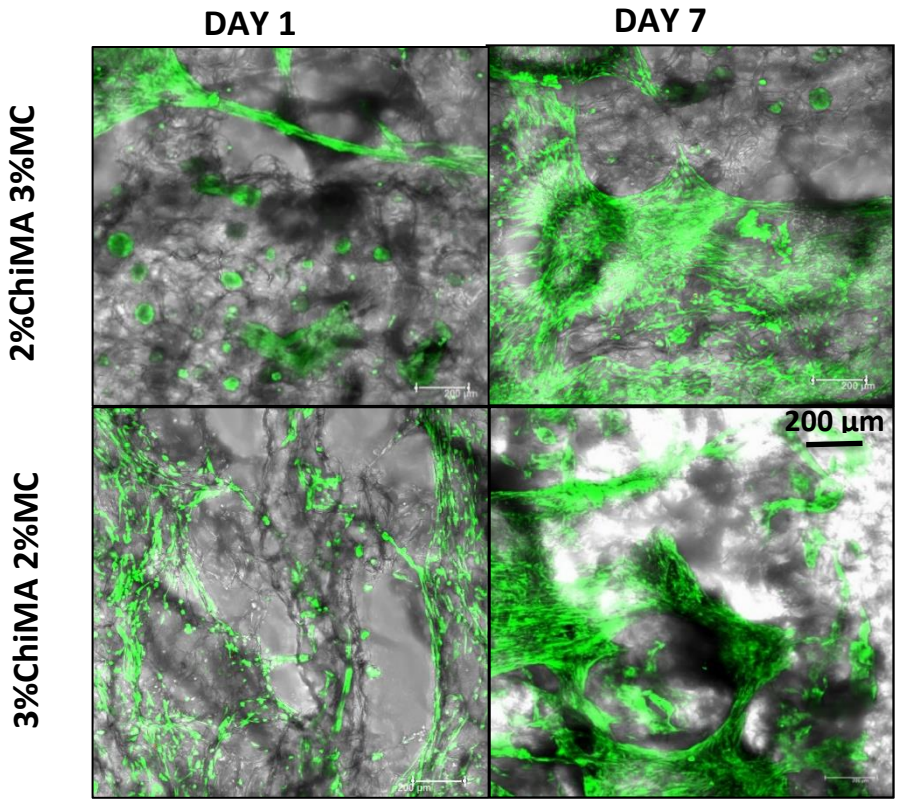


**Figure 3.27 Representative fluorescent images of HDFs cultured in 3D printed ChiMA/MC hydrogels at day 1 and day 7.**

# 4. CONCLUSION

Chitosan-based biomaterial inks were successfully developed and verified for its applicability as a feeding ink in extrusion-based bioprinting to create scaffolds to be used towards a wound healing application. Furthermore, the favourable properties to be expected in the scaffolds were also investigated.

A water soluble and photo-curable derivative of chitosan (ChiMA) was produced via methacrylation of the polymer chain, which was confirmed with $^{1}$H NMR and FTIR. Methyl cellulose was blended with ChiMA in different ratios to render it printable. Three main screening tests were used to identify the basic utility of formulated inks as biomaterials in would healing applications. The screening tests: initial screening by extrudability and semi-quantification assessment, were used as tools to identify the printable formulations. Although 6 ink formulations were deemed to be extrudable, only two formulations: 2% ChiMA/3%MC and 3% ChiMA/2%MC passed the semi-quantification assessment and showed possible properties of a well-suited biomaterial ink. The screening test was also used to explore some of the basic requirements and properties to be expected in the final scaffold. Thus, the findings are:

- Formulated biomaterial inks have instantaneous crosslinking ability upon UV exposure and reaches its maximum within 60s.
- Mechanical properties of the final hydrogels range between 7 KPa to 65 KPa, a suitable range to apply for highly anisotropic skin's different layers. Furthermore, the mechanical properties are amenable to manipulation by varying the crosslinking density. This could be achieved by using different photo-initiator concentrations and exposure

time.

- All the scaffolds possess a rapid rehydration property, which is useful in wound healing in terms of maintaining a moist environment and absorbing excess wound extrudates.
- From the two precursors that were used to synthesise the biomaterial, only ChiMA chains crosslink and MC remained as free polymer which can be released. This release of MC can create microchannels inside the scaffold and can be favourable for gaseous exchange and permeation of the nutrients.
- The developed hydrogel scaffolds can be degraded enzymatically but only up to a certain extent.

After acquiring a thorough understanding about the printable range and expected properties, two lead biomaterial inks were identified as promising materials and subjected to rheological assessment to confirm the suitable properties to be used as a biomaterial ink in extrusion-based printing. The two lead composite inks have well defined shear thinning behaviour and suitable yield stress values which are some of the key properties needed in extrusion bioprinting. Although MC is a thermo-responsive material, formulated biomaterial inks show independence from temperature. However, a temperature sweep test along with the crosslinking profile show the expected combined effect of ChiMA and MC as biomaterial ink; affording a higher G' at all times compared to ChiMA and MC themselves separately. As the final rheological evaluation, self-recovery ability was confirmed as shape fidelity of the printed structure would highly depend on it.

Development of a biomaterial ink as well as optimisation of it within existing printing operating parameters can be time consuming. A previously developed mathematical model was adapted which afforded a "Bioprinting window" for the two lead ink formulations. Apart from that, it

was also used to understand the capillary flow in terms of extrusion velocity, stress magnitude and duration. The findings are: 1) the shear rate inside the needle increases exponentially towards the needle wall. 2) highest stress with longest residence time and slowest extrusion velocity are shown at the needle wall. This data can be used to confirm the cytocompatibility of the extrusion printing and determine if this biomaterial would be conducive to cell printing as well.

Once the formulated inks were identified to have suitable rheological parameters as well, optimisation of the two lead biomaterial inks were carried out. According to the structure diameter evaluation with different printing speeds, 3% ChiMA/2%MC biomaterial ink shows better printing resolution compared to 2%ChiMA/3%MC biomaterial ink. This is also proven upon 8-layer printing where 3%ChiMA/2%MC biomaterial ink shows a better resolution with high shape fidelity. This is further supported by reproduction of different shapes comprising up to 8 layers with 3%ChiMA/2%MC biomaterial ink.

Finally, preliminary cytocompatibility studies were done using in-vitro cell culture of human dermal fibroblasts in 3D printed scaffolds. The scaffolds show no cytotoxicity but with poor cell attachment and limited cell proliferation. However, cell attachment and proliferation can be improved by a simple coating with collagen.

Through this study, a new biomaterial ink has been identified and added to the biomaterial ink data base. Chitosan-based biomaterial inks were formulated for the first time without using acidic or harsh chemicals. This newly developed biomaterial ink may open up new possibilities in biofabrication of structures for tissue engineering applications. Further studies of the scaffolds fabricate from the newly developed biomaterial can act as a bioactive wound dressing facilitating all the three wound healing stages.

# 5. FUTURE DIRECTIONS

The potential use of ChiMA/MC biomaterial ink in wound healing is promising. Here, as far as can be ascertained, this thesis work has developed, for the first time, a chitosan-based biomaterial ink which is environmentally and economically friendly. Further fundamental studies in several areas are needed before moving on to clinical trials.

Firstly, the crosslinking profile with different photo-initiators and different photo-initiator concentrations needs to be examined. This can also be correlated with the mechanical properties of the hydrogel as a way of manipulating the mechanical strength. As chitosan is also a promising biopolymer for the drug delivery application, further studies can be undertaken to study the incorporation of drugs and drug releasement related to wound healing (Saikia, Gogoi et al. 2015). A major focus in future studies should preferably be on exploring the anti-bacterial effect of the ChiMA as well as the ChiMA/MC biomaterial ink. Since the developed ChiMA/MC ink does not show strong interactions with cells, improvements can be done by modifying ChiMA with RDG peptides which are highly known to stimulate cell adhesion and proliferation (Hersel, Dahmen et al. 2003). Quantitative assays such as Celltiter Glo 3D (ATP activity) or MTS (mitochondrial metabolism) can be followed to get a better glimpse of the biology. Future work could be explored on introducing different polymers, instead of methyl cellulose, which are already used in wound healing, such as polyethylene glycol, glycine or hyaluronic acid etc.

# 6. REFERENCES


Abou-Zeid, N., et al. (2011). "Preparation, characterization and antibacterial properties of cyanoethylchitosan/cellulose acetate polymer blended films." Carbohydrate polymers **84**(1): 223-230.

Aderibigbe, B. and B. Buyana (2018). "Alginate in wound dressings." Pharmaceutics **10**(2): 42.

Altomare, L., et al. (2016). "Thermo-responsive methylcellulose hydrogels as temporary substrate for cell sheet biofabrication." Journal of Materials Science: Materials in Medicine **27**(5): 95.

Alves, N. and J. Mano (2008). "Chitosan derivatives obtained by chemical modifications for biomedical and environmental applications." International journal of biological macromolecules **43**(5): 401-414.

Aranaz, I., et al. (2009). "Functional characterization of chitin and chitosan." Current chemical biology **3**(2): 203-230.

Bayat, A., et al. (2003). "Skin scarring." Bmj **326**(7380): 88-92.

Bergamonti, L., et al. (2019). "3D printed chitosan scaffolds: A new TiO2 support for the photocatalytic degradation of amoxicillin in water." Water research **163**: 114841.

Boland, T., et al. (2006). "Application of inkjet printing to tissue engineering." Biotechnology journal **1**(9): 910-917.

Byrne, B. (2014). "Wound Management and Bandaging." ABC of Dermatology **241**: 197.

Chandika, P., et al. (2015). "Marine-derived biological macromolecule-based biomaterials for wound healing and skin tissue regeneration." International journal of biological macromolecules **77**: 24-35.

Chen, C.-H., et al. (2007). "Construction and characterization of fragmented mesenchymal-stem-cell sheets for intramuscular injection." Biomaterials **28**(31): 4643-4651.

Chimene, D., et al. (2016). "Advanced bioinks for 3D printing: a materials science perspective." Annals of biomedical engineering **44**(6): 2090-2102.

Chirani, N., et al. (2015). "History and applications of hydrogels." Journal of biomedical sciences **4**(2).

Chung, J. H., et al. (2013). "Bio-ink properties and printability for extrusion printing living cells." Biomaterials Science **1**(7): 763-773.

Collage, O. (2014). Anatomy & Physiology, OpenStax CNX.

Cui, X., et al. (2012). "Thermal inkjet printing in tissue engineering and regenerative medicine." Recent patents on drug delivery & formulation **6**(2): 149-155.

Diegelmann, R. F. and M. C. Evans (2004). "Wound healing: an overview of acute, fibrotic and delayed healing." Front Biosci **9**(1): 283-289.

Dinoro, J. N. (2016). "3D printing PhycoTrix™ for wound healing."

Diolosà, M., et al. (2014). "Use of methacrylate-modified chitosan to increase the durability of dentine bonding systems." Biomacromolecules **15**(12): 4606-4613.

Doillon, C., et al. (1986). "Collagen-based wound dressings: Control of the pore structure and morphology." Journal of Biomedical Materials Research Part A **20**(8): 1219-1228.

Drury, J. L. and D. J. Mooney (2003). "Hydrogels for tissue engineering: scaffold design variables and applications." Biomaterials **24**(24): 4337-4351.

Eltom, A., et al. (2019). "Scaffold Techniques and Designs in Tissue Engineering Functions and Purposes: A Review." Advances in Materials Science and Engineering **2019**.

Enoch, S. and D. J. Leaper (2008). "Basic science of wound healing." Surgery (Oxford) **26**(2): 31-37.

Fedorovich, N. E., et al. (2007). "Hydrogels as extracellular matrices for skeletal tissue engineering: state-of-the-art and novel application in organ printing." Tissue engineering **13**(8): 1905-1925.

Fei Liu, X., et al. (2001). "Antibacterial action of chitosan and carboxymethylated chitosan." Journal of applied polymer science **79**(7): 1324-1335.

Fernandes Queiroz, M., et al. (2014). "Does the use of chitosan contribute to oxalate kidney stone formation?" Marine drugs **13**(1): 141-158.

Flanagan, M. (2000). "The physiology of wound healing." Journal of wound care **9**(6): 299-300.

Freinkel, R. K. and D. T. Woodley (2001). The biology of the skin, CRC Press.

Gaharwar, A. K., et al. (2013). "Photocrosslinked nanocomposite hydrogels from PEG and silica nanospheres: structural, mechanical and cell adhesion characteristics." Materials Science and Engineering: C **33**(3): 1800-1807.

Gansau, J. and C. Buckley (2018). "Incorporation of Collagen and Hyaluronic Acid to Enhance the Bioactivity of Fibrin-Based Hydrogels for Nucleus Pulposus Regeneration." Journal of functional biomaterials **9**(3): 43.

Gao, T., et al. (2018). "Optimization of gelatin–alginate composite bioink printability using rheological parameters: a systematic approach." Biofabrication **10**(3): 034106.

Gopinathan, J. and I. Noh (2018). "Recent trends in bioinks for 3D printing." Biomaterials

research **22**(1): 11.

Groll, J., et al. (2018). "A definition of bioinks and their distinction from biomaterial inks." Biofabrication **11**(1): 013001.

Gu, Z., et al. (2019). "Development of 3D Bioprinting: From Printing Methods to Biomedical Applications."

Guarino, V., et al. (2015). "Degradation properties and metabolic activity of alginate and chitosan polyelectrolytes for drug delivery and tissue engineering applications."

Guillotin, B. and F. Guillemot (2011). "Cell patterning technologies for organotypic tissue fabrication." Trends in biotechnology **29**(4): 183-190.

Guillotin, B., et al. (2010). "Laser assisted bioprinting of engineered tissue with high cell density and microscale organization." Biomaterials **31**(28): 7250-7256.

Guo, S. a. and L. A. DiPietro (2010). "Factors affecting wound healing." Journal of dental research **89**(3): 219-229.

Guvendiren, M., et al. (2012). "Shear-thinning hydrogels for biomedical applications." Soft matter **8**(2): 260-272.

Habibi, Y., et al. (2010). "Cellulose nanocrystals: chemistry, self-assembly, and applications." Chemical reviews **110**(6): 3479-3500.

Han, G. and R. Ceilley (2017). "Chronic wound healing: a review of current management and treatments." Advances in therapy: 1-12.

Han, T., et al. (2012). "Methods of N-acetylated chitosan scaffolds and its in-vitro biodegradation by lysozyme." Journal of Biomedical Science and Engineering **5**(01): 15.

Hankiewicz, J. and E. Swierczek (1974). "Lysozyme in human body fluids." Clinica chimica acta **57**(3): 205-209.

Harkins, A. L., et al. (2014). "Chitosan–cellulose composite for wound dressing material. Part 2. Antimicrobial activity, blood absorption ability, and biocompatibility." Journal of Biomedical Materials Research Part B: Applied Biomaterials **102**(6): 1199-1206.

Hersel, U., et al. (2003). "RGD modified polymers: biomaterials for stimulated cell adhesion and beyond." Biomaterials **24**(24): 4385-4415.

Highley, C. B., et al. (2015). "Direct 3D printing of shear-thinning hydrogels into self-healing hydrogels." Advanced Materials **27**(34): 5075-5079.

Hoffman, A. S. (2012). "Hydrogels for biomedical applications." Advanced drug delivery reviews **64**: 18-23.

Hölzl, K., et al. (2016). "Bioink properties before, during and after 3D bioprinting." Biofabrication **8**(3): 032002.

HPS, A. K., et al. (2016). "A review on chitosan-cellulose blends and nanocellulose reinforced chitosan biocomposites: Properties and their applications." Carbohydrate polymers **150**: 216-226.

Hu, J., et al. (2012). "Visible light crosslinkable chitosan hydrogels for tissue engineering." Acta biomaterialia **8**(5): 1730-1738.

Huang, Z.-M., et al. (2003). "A review on polymer nanofibers by electrospinning and their applications in nanocomposites." Composites science and technology **63**(15): 2223-2253.

Hubbe, M. A., et al. (2008). "Cellulosic nanocomposites: a review." BioResources **3**(3): 929-980.

Ikada, Y. (2006). "Challenges in tissue engineering." Journal of The Royal Society Interface **3**(10): 589-601.

Janmey, P. A. and R. T. Miller (2011). "Mechanisms of mechanical signaling in development and disease." J Cell Sci **124**(1): 9-18.

Jungst, T., et al. (2015). "Strategies and molecular design criteria for 3D printable hydrogels." Chemical reviews **116**(3): 1496-1539.

Kalia, S., et al. (2011). "Cellulose-based bio-and nanocomposites: a review." International Journal of Polymer Science **2011**.

Kalra, A., et al. (2016). "Mechanical behaviour of skin: a review." J. Mater. Sci. Eng **5**(4): 1000254.

Kasaai, M. R. (2010). "Determination of the degree of N-acetylation for chitin and chitosan by various NMR spectroscopy techniques: A review." Carbohydrate polymers **79**(4): 801-810.

Khalili, A. and M. Ahmad (2015). "A review of cell adhesion studies for biomedical and biological applications." International journal of molecular sciences **16**(8): 18149-18184.

Kim, S. H., et al. (2018). "Precisely printable and biocompatible silk fibroin bioink for digital light processing 3D printing." Nature communications **9**(1): 1620.

Kumar, M. R., et al. (2004). "Chitosan chemistry and pharmaceutical perspectives." Chemical reviews **104**(12): 6017-6084.

Kyle, S., et al. (2017). "'Printability'of Candidate Biomaterials for Extrusion Based 3D Printing: State-of-the-Art." Advanced healthcare materials **6**(16): 1700264.

Lavertu, M., et al. (2003). "A validated 1H NMR method for the determination of the degree of deacetylation of chitosan." Journal of pharmaceutical and biomedical analysis **32**(6): 1149-1158.

Law, N., et al. (2018). "Characterisation of hyaluronic acid methylcellulose hydrogels for 3D

bioprinting." Journal of the mechanical behavior of biomedical materials **77**: 389-399.

Lazarus, G. S., et al. (1994). "Definitions and guidelines for assessment of wounds and evaluation of healing." Wound Repair and Regeneration **2**(3): 165-170.

Li, H., et al. (2016). "Rheological study on 3D printability of alginate hydrogel and effect of graphene oxide." **2**(2).

Li, L., et al. (2001). "Gel network structure of methylcellulose in water." Langmuir **17**(26): 8062-8068.

Liang, D., et al. (2007). "Functional electrospun nanofibrous scaffolds for biomedical applications." Advanced drug delivery reviews **59**(14): 1392-1412.

Liu, Z., et al. (2019). "Linking rheology and printability of a multicomponent gel system of carrageenan-xanthan-starch in extrusion based additive manufacturing." Food Hydrocolloids **87**: 413-424.

Lo, D. D., et al. (2015). Differences in Foetal, Adult Skin and Mucosal Repair. Stem Cell Biology and Tissue Engineering in Dental Sciences, Elsevier**:** 691-702.

Malda, J., et al. (2013). "25th anniversary article: engineering hydrogels for biofabrication." Advanced materials **25**(36): 5011-5028.

Mandal, B. B. and S. C. Kundu (2008). "Non-bioengineered silk fibroin protein 3D scaffolds for potential biotechnological and tissue engineering applications." Macromolecular bioscience **8**(9): 807-818.

Marshall, C. D., et al. (2018). "Cutaneous scarring: Basic science, current treatments, and future directions." Advances in wound care **7**(2): 29-45.

McKee, C. T., et al. (2011). "Indentation versus tensile measurements of Young's modulus for soft biological tissues." Tissue Engineering Part B: Reviews **17**(3): 155-164.

Menger, F. M. and A. V. Peresypkin (2003). "Strings of vesicles: flow behavior in an unusual type of aqueous gel." Journal of the American Chemical Society **125**(18): 5340-5345.

Metcalfe, A. D. and M. W. Ferguson (2007). "Bioengineering skin using mechanisms of regeneration and repair." Biomaterials **28**(34): 5100-5113.

Mironov, V., et al. (2009). "Biofabrication: a 21st century manufacturing paradigm." Biofabrication **1**(2): 022001.

Montembault, A., et al. (2005). "Physico-chemical studies of the gelation of chitosan in a hydroalcoholic medium." Biomaterials **26**(8): 933-943.

Morton, L. M. and T. J. Phillips (2016). "Wound healing and treating wounds: Differential diagnosis and evaluation of chronic wounds." Journal of the American Academy of Dermatology **74**(4): 589-605.

Müller, M., et al. (2015). "Nanostructured Pluronic hydrogels as bioinks for 3D bioprinting." Biofabrication **7**(3): 035006.

Murphy, P. S. and G. R. Evans (2012). "Advances in wound healing: a review of current wound healing products." Plastic surgery international **2012**.

Murphy, S. V. and A. Atala (2014). "3D bioprinting of tissues and organs." Nature biotechnology **32**(8): 773.

Muzzarelli, R. (1997). "Human enzymatic activities related to the therapeutic administration of chitin derivatives." Cellular and Molecular Life Sciences CMLS **53**(2): 131-140.

Naficy, S., et al. (2009). "Modulated release of dexamethasone from chitosan–carbon nanotube films." Sensors and Actuators A: Physical **155**(1): 120-124.

Nakamura, M., et al. (2006). Inkjet bioprinting as an effective tool for tissue fabrication. NIP & Digital Fabrication Conference, Society for Imaging Science and Technology.

Negrini, N. C., et al. (2018). "3D printing of methylcellulose-based hydrogels." Bioprinting **10**: e00024.

Ning, L. and X. Chen (2017). "A brief review of extrusion-based tissue scaffold bio-printing." Biotechnology Journal.

O'sullivan, A. C. (1997). "Cellulose: the structure slowly unravels." Cellulose **4**(3): 173-207.

Ouyang, L., et al. (2016). "Effect of bioink properties on printability and cell viability for 3D bioplotting of embryonic stem cells." Biofabrication **8**(3): 035020.

Ozbolat, I. T. and M. Hospodiuk (2016). "Current advances and future perspectives in extrusion-based bioprinting." Biomaterials **76**: 321-343.

Pacella, R. (2017). "Chronic Wounds in Australia."

Paul, W. and C. P. Sharma (2004). "Chitosan and alginate wound dressings: a short review." Trends Biomater Artif Organs **18**(1): 18-23.

Paxton, N., et al. (2017). "Proposal to assess printability of bioinks for extrusion-based bioprinting and evaluation of rheological properties governing bioprintability." Biofabrication **9**(4): 044107.

Peltola, S. M., et al. (2008). "A review of rapid prototyping techniques for tissue engineering purposes." Annals of medicine **40**(4): 268-280.

Pignatello, R. (2013). Advances in biomaterials science and biomedical applications, BoD–Books on Demand.

Rabea, E. I., et al. (2003). "Chitosan as antimicrobial agent: applications and mode of action." Biomacromolecules **4**(6): 1457-1465.

Ren, D., et al. (2005). "The enzymatic degradation and swelling properties of chitosan matrices with different degrees of N-acetylation." Carbohydrate Research **340**(15): 2403-2410.

Rhett, J. M., et al. (2008). "Novel therapies for scar reduction and regenerative healing of skin wounds." Trends in biotechnology **26**(4): 173-180.

Rinaudo, M. (2006). "Chitin and chitosan: properties and applications." Progress in polymer science **31**(7): 603-632.

Saikia, C., et al. (2015). "Chitosan: A promising biopolymer in drug delivery applications." J. Mol. Genet. Med. S **4**(006).

Sayyar, S., et al. (2017). "3D printable conducting hydrogels containing chemically converted graphene." Nanoscale **9**(5): 2038-2050.

Schütz, K., et al. (2017). "Three-dimensional plotting of a cell-laden alginate/methylcellulose blend: towards biofabrication of tissue engineering constructs with clinically relevant dimensions." Journal of tissue engineering and regenerative medicine **11**(5): 1574-1587.

Sears, N. A., et al. (2016). "A review of three-dimensional printing in tissue engineering." Tissue Engineering Part B: Reviews **22**(4): 298-310.

Shevchenko, R. V., et al. (2009). "A review of tissue-engineered skin bioconstructs available for skin reconstruction." Journal of the Royal Society Interface: rsif20090403.

Silva, J. M., et al. (2016). "Biomimetic extracellular environment based on natural origin polyelectrolyte multilayers." Small **12**(32): 4308-4342.

Singh, S., et al. (2017). "The physiology of wound healing." Surgery-Oxford International Edition **35**(9): 473-477.

Siqueira, G., et al. (2017). "Cellulose nanocrystal inks for 3D printing of textured cellular architectures." Advanced Functional Materials **27**(12): 1604619.

Skardal, A. and A. Atala (2015). "Biomaterials for integration with 3-D bioprinting." Annals of biomedical engineering **43**(3): 730-746.

Smith, L. A., et al. (2007). "Nanofibrous scaffolds and their biological effects." Nanotechnologies for the Life Sciences: Online.

Snyder, J., et al. (2011). "Bioprinting cell-laden matrigel for radioprotection study of liver by pro-drug conversion in a dual-tissue microfluidic chip." Biofabrication **3**(3): 034112.

Snyder, J., et al. (2015). "Mesenchymal stem cell printing and process regulated cell properties." Biofabrication **7**(4): 044106.

Subia, B., et al. (2010). "Biomaterial scaffold fabrication techniques for potential tissue engineering applications." Tissue engineering **141**.

Suntornnond, R., et al. (2016). "A mathematical model on the resolution of extrusion bioprinting for the development of new bioinks." Materials **9**(9): 756.

Tibbitt, M. W. and K. S. Anseth (2009). "Hydrogels as extracellular matrix mimics for 3D cell culture." Biotechnology and bioengineering **103**(4): 655-663.

Tran, C. D., et al. (2013). "Recyclable synthesis, characterization, and antimicrobial activity of chitosan-based polysaccharide composite materials." Journal of Biomedical Materials Research Part A **101**(8): 2248-2257.

Wu, Q., et al. (2018). "Processing and properties of chitosan Inks for 3D printing of hydrogel microstructures." ACS Biomaterials Science & Engineering **4**(7): 2643-2652.

Xiang, Z., et al. (2006). "Collagen–GAG scaffolds grafted onto myocardial infarcts in a rat model: a delivery vehicle for mesenchymal stem cells." Tissue engineering **12**(9): 2467-2478.

Yan, W.-C., et al. (2018). "3D bioprinting of skin tissue: From pre-processing to final product evaluation." Advanced drug delivery reviews **132**: 270-295.

Yang, T. (2012). Mechanical and swelling properties of hydrogels, KTH Royal Institute of Technology.

Yates, C. C., et al. (2012). "Skin wound healing and scarring: fetal wounds and regenerative restitution." Birth Defects Research Part C: Embryo Today: Reviews **96**(4): 325-333.

Ye, K., et al. (2014). "Chondrogenesis of infrapatellar fat pad derived adipose stem cells in 3D printed chitosan scaffold." PloS one **9**(6): e99410.

You, F., et al. (2017). "Application of extrusion-based hydrogel bioprinting for cartilage tissue engineering." International journal of molecular sciences **18**(7): 1597.

Yu, L. M., et al. (2007). "Peptide surface modification of methacrylamide chitosan for neural tissue engineering applications." Journal of Biomedical Materials Research Part A **82**(1): 243-255.

Zahedi, P., et al. (2010). "A review on wound dressings with an emphasis on electrospun nanofibrous polymeric bandages." Polymers for Advanced Technologies **21**(2): 77-95.

Zhang, J., et al. (2019). "Silk particles, microfibres and nanofibres: A comparative study of their functions in 3D printing hydrogel scaffolds." Materials Science and Engineering: C: 109784.

Zhang, S. (2003). "Fabrication of novel biomaterials through molecular self-assembly." Nature biotechnology **21**(10): 1171.

Zhao, P., et al. (2018). "Fabrication of scaffolds in tissue engineering: A review." Frontiers of Mechanical Engineering **13**(1): 107-119.

Zhu, L. and K. M. Bratlie (2018). "pH sensitive methacrylated chitosan hydrogels with tunable physical and chemical properties." Biochemical engineering journal **132**: 38-46.